

SPECTROSCOPIC STUDY OF Dy<sup>3+</sup> DOPED Gd<sub>2</sub>O<sub>3</sub> – B<sub>2</sub>O<sub>3</sub> GLASS FOR  
PHOTONIC AND SCINTILLATION MATERIALS



A Thesis Submitted in Partial Fulfillment of the Requirements for the  
Degree of Doctor of Philosophy in Applied Physics  
Suranaree University of Technology  
Academic Year 2022

การศึกษาเชิงสเปกโทรสโกปีของแก้ว  $Gd_2O_3 - B_2O_3$  ที่เจือด้วย  $Dy^{3+}$   
สำหรับเป็นวัสดุโฟโตนิกส์และซินทิลเลชัน



วิทยานิพนธ์นี้เป็นส่วนหนึ่งของการศึกษาตามหลักสูตรปริญญาวิทยาศาสตรดุษฎีบัณฑิต  
สาขาวิชาฟิสิกส์ประยุกต์  
มหาวิทยาลัยเทคโนโลยีสุรนารี  
ปีการศึกษา 2565

SPECTROSCOPIC STUDY OF Dy<sup>3+</sup> DOPED Gd<sub>2</sub>O<sub>3</sub>-B<sub>2</sub>O<sub>3</sub> GLASS FOR  
PHOTONIC AND SCINTILLATION MATERIALS

Suranaree University of Technology has approved this thesis submitted in partial fulfillment of the requirements for a Degree of Doctor of Philosophy.

Thesis Examining Committee

Rattikorn Yimnirun

(Prof. Dr. Rattikorn Yimnirun)

Chairperson

P. Manyum

(Assoc. Prof. Dr. Prapan Manyum)

Member (Thesis Advisor)

A. Kaewkhao

(Assoc. Prof. Dr. Jakrapong Kaewkhao)

Member

Narit Triamnak

(Asst. Prof. Dr. Narit Triamnak)

Member

Natthapong Wongdamnern

(Dr. Natthapong Wongdamnern)

Member

Chatchai Jothityangkoon

(Assoc. Prof. Dr. Chatchai Jothityangkoon)  
Vice Rector for Academic Affairs  
and Quality Assurance

Santi Maensiri

(Prof. Dr. Santi Maensiri)  
Dean of Institute of Science

อัจฉริยศาสตร์ ผงชา : การศึกษาเชิงสเปกโทรสโกปีของแก้ว  $Gd_2O_3 - B_2O_3$  ที่เจือด้วย  $Dy^{3+}$  สำหรับเป็นวัสดุโฟโตนิกส์และซินทิลเลชัน (SPECTROSCOPIC STUDY OF  $Dy^{3+}$  DOPED  $Gd_2O_3 - B_2O_3$  GLASS FOR PHOTONIC AND SCINTILLATION MATERIALS)  
อาจารย์ที่ปรึกษา : รองศาสตราจารย์ ดร.ประพันธ์ แม่นยำ, 46 หน้า.

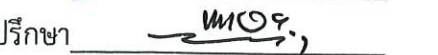
คำสำคัญ: ดิสโพลีเมอร์, แก้ว, สมบัติทางกายภาพ, สมบัติทางแสง, โฟโตนิกส์, ซินทิลเลชัน

งานวิจัยนี้มีจุดประสงค์เพื่อศึกษาพฤติกรรมการเรืองแสงและการประยุกต์ใช้งานจากระบบ แก้วแกดโดลิเนียมบอเรตจากสูตร  $27.5Gd_2O_3-(72.5-x)B_2O_3-xDy_2O_3$  โดยการเจือด้วยแร่โลหะหายาก ไทรวาเลนซ์ออกไซด์ ดิสโพลีเมอร์ ( $Dy^{3+}$ ) และเปลี่ยนแปลงปริมาณความเข้มข้นของดิสโพลีเมอร์ (x) เป็น 0.05, 0.1, 0.5, 1.0 และ 1.5 ร้อยละโดยโมล ตามลำดับ โดยแก้วถูกเตรียมขึ้นด้วยเทคนิค การหลอมที่อุณหภูมิ 1,400 องศาเซลเซียส และทำให้เย็นตัวลงอย่างรวดเร็ว โดยในงานนี้แบ่ง การศึกษาเป็น 2 ส่วนคือ 1. การออกแบบการห่อหุ้มแอลอีดี และ 2. การออกแบบระบบการ ตรวจสอบการถ่ายภาพวัสดุด้วยรังสีเอกซ์ โดยทั่วไป WLED ประกอบด้วย 3 ส่วน คือ 1. แผ่น LED chip (InGaN) 2. ชั้นเคลือบด้วยสารฟอสฟอรัส (Yag:Ce) และ 3. ชั้นห่อหุ้มด้วย Epoxy Resin อย่างไรก็ตามเนื่องจาก Epoxy Resin มีข้อเสีย คือ เป็นพิษ และอายุการใช้งานค่อนข้างสั้น ดังนั้นงานวิจัยนี้ จึงได้มีแนวคิดเปลี่ยนวัสดุตัวห่อหุ้มจากเดิมที่เป็นการใช้สารฟอสฟอรัส และ Epoxy Resin เคลือบด้าน ในเป็นวัสดุชนิดแก้ว เนื่องจากแก้วสามารถทำหน้าที่เป็นเปลือกห่อหุ้มเซมิคอนดักเตอร์และสามารถ ขึ้นรูปได้หลากหลายรูปทรง นอกจากนี้ยังสามารถนำข้อดีของแก้วมาประยุกต์ต่อยอด เพื่อยืนยันใน การนำมาใช้งานจริง จึงได้ศึกษาคุณสมบัติทางแสงโดยใช้ อิเล็กโตรลูมิเนสเซนส์ ซึ่งจากผลการศึกษา การนำแก้วมาประยุกต์ใช้ พบว่าแก้วสามารถใช้สำหรับการห่อหุ้มแอลอีดี (LED) และยังเพิ่ม ประสิทธิภาพความสว่าง 90% จากความสว่างตั้งต้น นอกจากนี้ งานวิจัยได้ศึกษาและออกแบบระบบ สำหรับการถ่ายภาพเอกซเรย์ที่ใช้ต้นทุนต่ำ และคุณภาพสูง โดยใช้แก้วที่สังเคราะห์มาเป็นวัสดุซินทิล เลชัน อุปกรณ์นี้สามารถตรวจสอบสารอินทรีย์ผลึกเดี่ยวเพื่อแปลงรังสีไอออไนซ์ให้เป็นแสงในช่วง ความยาวคลื่นที่ตามองเห็นได้ (400 -700 นาโนเมตร) ดังนั้นระบบนี้ สามารถที่จะใช้ในการวัด ทางด้านรังสี และการวิเคราะห์การถ่ายภาพ x-ray ของตัวอย่างในทางการแพทย์ได้

สาขาวิชาฟิสิกส์  
ปีการศึกษา 2565

ลายมือชื่อนักศึกษา

ลายมือชื่ออาจารย์ที่ปรึกษา

ATCHARIYASART PHONGSA : SPECTROSCOPIC STUDY OF  $Dy^{3+}$  DOPED  $Gd_2O_3 - B_2O_3$  GLASS FOR PHOTONIC AND SCINTILLATION MATERIALS. THESIS ADVISOR : ASSOC. PROF. PRAPAN MANYUM, Ph.D. 49 PP.

Keyword: Dysprosium, Glass, Physical Properties, Optical Properties, Photonics, Scintillation

This work aimed to explore luminescence properties and application of the gadolinium borate glass system. The chemical composition was  $27.5Gd_2O_3-(72.5-x)B_2O_3-xDy_2O_3$  which dysprosium oxide is the rare earth trivalent. Variations in the concentrations of  $Dy^{3+}$  ion used are 0.05, 0.1, 0.5, 1.0 and 1.5 mol%. This glass was prepared by melt-quenching technique at  $1.400\text{ }^\circ\text{C}$  for 3 hours. This work divides the study into two parts: 1. WLED encapsulation design and 2. Design the X-ray imaging system. W-LED usually has three main parts: 1. LED chip (InGaN) 2. Phosphor-coated (YAG: Ce) layer and 3. LED encapsulation by epoxy resin. Unfortunately, epoxy resin has disadvantages such as toxicity and short decay time, so this motivates us to adopt a challenging design by replacing epoxy resin encapsulation with glass samples. Instead of using the original phosphor coating and epoxy resin, the glass sample can efficiently act as an encapsulating shell with a semiconductor material. The glass samples can also be varied with various shapes and optimize the LED encapsulation's brightness. Therefore, the researcher has applied the advantages of glass to further application by designing an inverted bell shape. Moreover, the optical properties were studied using Electroluminescence (EL) to ensure that this glass can be used as an LED encapsulation. A new system with low-cost fabrication and high-quality x-ray scintillation material-based imaging systems was also designed. The device utilizes a single-crystal inorganic scintillator to convert ionizing radiation to visible light wavelengths (400 -700 nm). It also can be used to measure radiation and x-ray imaging analysis of medical samples.

School of Physics  
Academic Year 2022

Student's Signature Atchariyasart P.  
Advisor's Signature Prapan Manyum,

## ACKNOWLEDGEMENTS

This thesis could not be completed without the help and support of many people, for which I express my sincere gratitude.

I would like to thank Assoc. Prof. Dr. Panomsak Meemon accepted me to study for the Ph.D. and allowed me to carry out research in the field of funding together with some optics funding and supporting from 2016 to 2021.

I want to express my sincere gratitude to my thesis advisor, Assoc. Prof. Dr. Prapan Manyum, provided me the guidance, support, and excellent opportunities to carry out this research activity.

I would like to thank Asst. Prof. Dr. Rattikorn Yimnirand, Chairman of the Thesis Defense Examination Committee who provides supporting and advice/suggestions on research and science in various fields.

I would like to thank Assoc. Prof. Dr. Jakrapong Kaewkhao, who is also one of the thesis defense committee members for giving me a scholarship and an opportunity to carry my research in his laboratory the Center of Excellence in Glass Technology and Materials Science (CEGM).

I would like to thank Asst. Prof. Dr. Narit Trimnak member of the thesis defense committee who help me with everything in Nakhon Pathom.

I would like to thank Dr. Dr. Natthapong Wongdamnern who is the thesis defense committee, for assistance and guidance in the research writing.

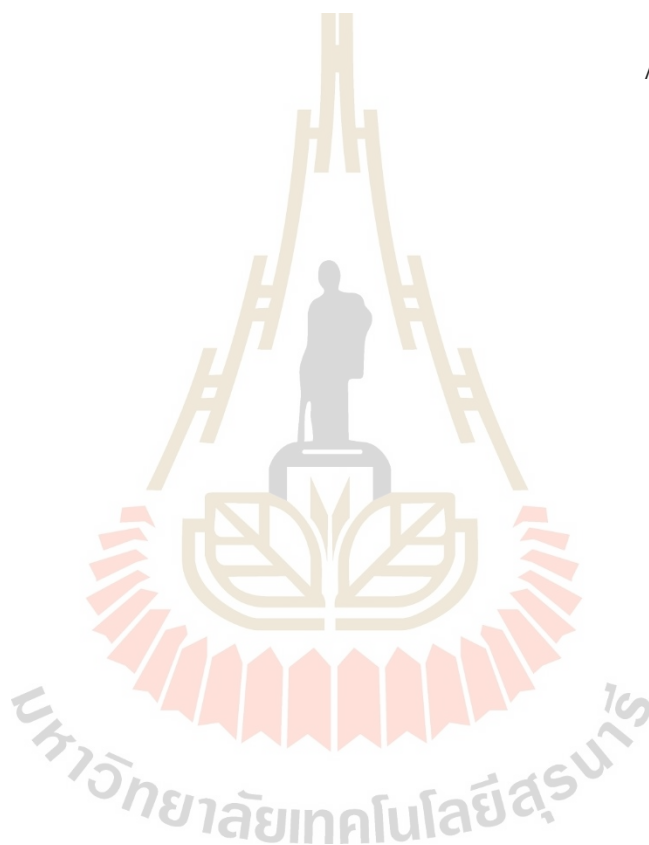
I would like to give big thank to Dr. Nuantip Wantana , Dr. Wipakorn Rittisut, Ms.Chayani S. Sarumaha, and Dr. R. Rajaramakrishna of the Glass group and Yimnirun group, school of physics, SUT, and Nakhon Pathom Rajabhat University (NPRU) ,all teachers, my friends, my seniors, my juniors, and all staffs in school of Physics, SUT for their support.

I would like to thank the National Research Council of Thailand (NRCT) for funding. J. Kaewkhao would like to thanks National Research Council of Thailand (NRCT) under Research Grants for Talented Mid-Career Researchers Project. I would like to

express their gratitude to W. Rittisut and N. Wantana for their assistance with the measurements. These studies were also supported by the National Nanotechnology Center's (NANOTEC) Research Network NANOTEC (RNN) program, NSTDA, Suranaree University of Technology's Center for Scientific and Technological Equipment, and Thailand's Synchrotron Light Research Institute (Public Organization).

Finally, I want to express appreciation to my parents, and my sisters for their tremendous love, support and encouragement.

Atchariyasart Phongsa



# CONTENTS

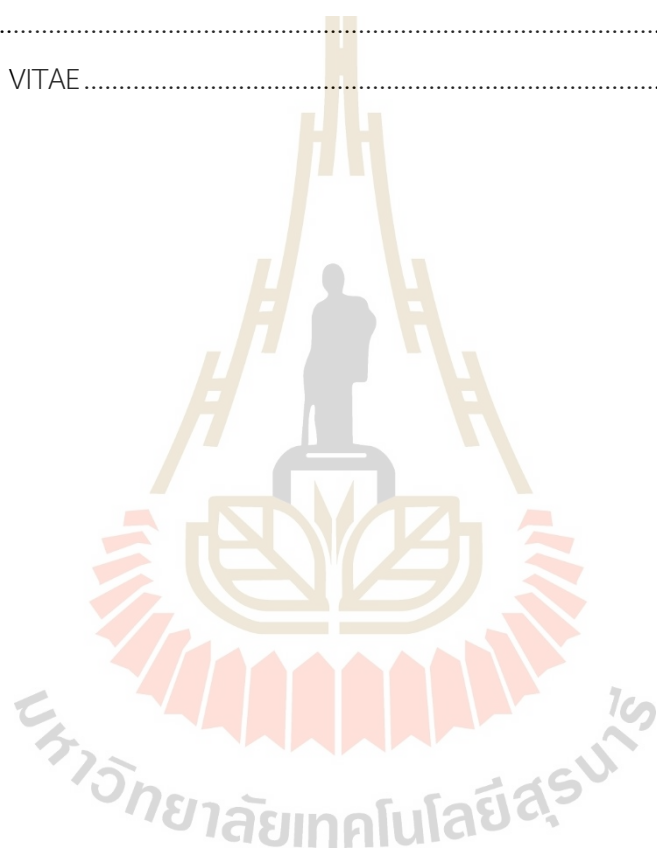
	Page
ABSTRACT IN THAI.....	I
ABSTRACT IN ENGLISH.....	II
ACKNOWLEDGEMENTS.....	III
CONTENTS.....	V
LIST OF TABLES .....	VIII
LIST OF FIGURES .....	IX
<b>CHAPTER</b>	
<b>I INTRODUCTION.....</b>	<b>1</b>
1.1 Background and motivation.....	1
1.2 Objectives of the thesis.....	4
1.3 Outline of the thesis .....	4
<b>II THEORY AND LITERATURE REVIEW.....</b>	<b>6</b>
2.1 Inorganic light-emitting diodes (leds).....	6
2.2 White and colored leds.....	7
2.3 Phosphor-converted leds.....	9
2.4 Composition of the present glass.....	11
2.4.1 Borate ( $B_2O_3$ ) .....	13
2.4.2 Gadolinium oxides ( $Gd_2O_3$ ).....	13
2.4.3 Dysprosium oxides ( $Dy_2O_3$ ).....	14
2.5 Glass forming networks.....	14
2.5.1 Network formers .....	14
2.5.2 Intermediate.....	14
2.5.3 Network modifiers.....	15
2.6 Lanthanides.....	15

## CONTENTS (Continued)

		Page
	2.7 CIE Chromaticity coordination and color correlated temperatur (CCT) .....	17
	2.8 Scintillation.....	17
<b>III</b>	<b>RESEARCH METHODOLOGY .....</b>	<b>20</b>
	3.1 Sample preparation .....	20
	3.1.1 Preparation of Dy <sub>2</sub> O <sub>3</sub> doped (host glass).....	20
	3.2 Physical properties .....	21
	3.2.1 The density & Molar volumes .....	21
	3.2.2 Refractive index.....	22
	3.3 Structural properties .....	23
	3.3.1 X-ray diffraction.....	23
	3.4 Optical and spectral properties.....	24
	3.4.1 Fourier-transform infrared spectroscopy .....	24
	3.4.2 UV-Visible spectrophotometer .....	25
	3.4.3 Photoluminescence technique .....	26
	3.4.4 X-ray induced luminescence technique .....	27
	3.4.5 Electroluminescent.....	27
<b>IV</b>	<b>RESULTS AND DISCUSSION .....</b>	<b>29</b>
	4.1 27.5GD <sub>2</sub> O <sub>3</sub> -(72.5-X) B <sub>2</sub> O <sub>3</sub> -XDy <sub>2</sub> O <sub>3</sub> GLASS SYSTEM.....	29
	4.4.1 Structural properties of glass.....	29
	4.4.2 Physical properties .....	30
	4.4.3 Fourier Transform Infrared Spectroscopy (FTIR).....	32
	4.4.4 UV-vis-NIR Spectrophotometer .....	33
	4.4.5 Absorption Spectra .....	34
	4.4.6 Energy Transfer .....	36
	4.4.7 Photoluminescence excitation and emission (PLEs) spectra.....	36
	4.4.8 Decay Time .....	38

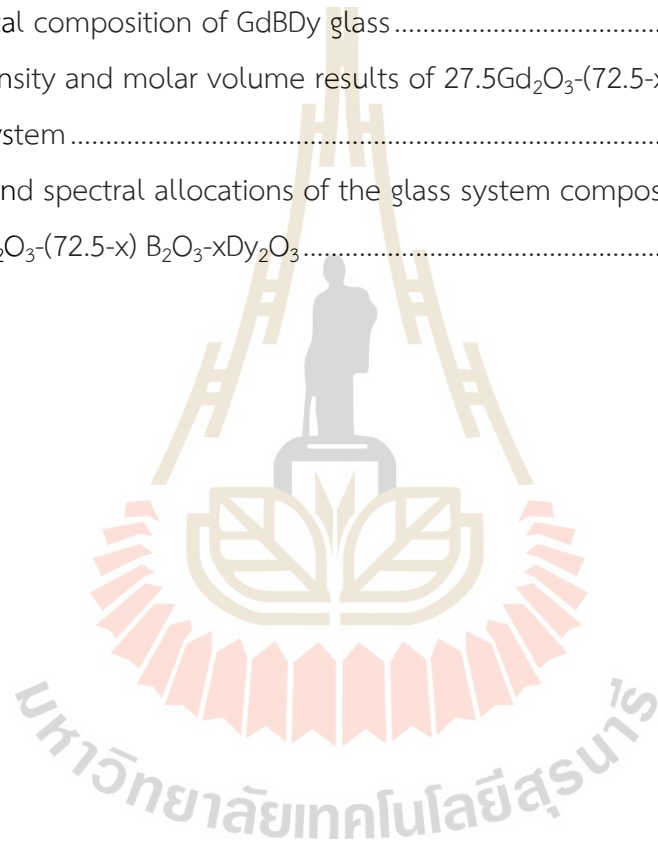
## CONTENT (Continued)

	Page
4.4.9 CIE chromaticity coordinates and color correlated temperature (CCT).....	39
4.4.10 Application of Blue LED Encapsulation .....	39
<b>V CONCLUSIONSION</b> .....	41
REFERENCES .....	42
CURRICULUM VITAE.....	47



## LIST OF TABLES

Table	Page
2.1 Comparison of advantages and disadvantages of LED.....	11
2.2 Electron configuration of lanthanide elements and ions.....	16
3.1 Chemical composition of GdBdY glass.....	20
4.1 The density and molar volume results of $27.5\text{Gd}_2\text{O}_3-(72.5-x)\text{B}_2\text{O}_3-x\text{Dy}_2\text{O}_3$ glass system.....	31
4.2 FTIR band spectral allocations of the glass system composed of $27.5\text{Gd}_2\text{O}_3-(72.5-x)\text{B}_2\text{O}_3-x\text{Dy}_2\text{O}_3$ .....	33



## LIST OF FIGURES

Figure	Page
1.1 The timeline of major discoveries in modern lighting technologies(Adapt-form: GE History, the history of the LED, OSRAM, and Lengthening the day).....	3
2.1 LEDs with a traditional 5-millimeter diameter (on the left) and an LED with a high-power lighting.....	7
2.2 Summary of different concepts to generate white light by primary light sources.....	7
2.3 The typical spectrum of a blue InGaN LED, a green InGaN LED, and a red AlGaInP LED (ranging from $x = 0.0$ to about 0.45).....	8
2.4 InGaP LED shaped as a truncated inverted pyramid for efficient light extraction .....	9
2.5 Emission spectra of a white LED comprising a 460 nm-emitting blue InGaN chip and a phosphor as a function of the optical thickness of the YAG:Ce layer.....	10
2.6 The volume-temperature diagram for a glass-forming liquid.....	12
2.7 A schematic representation of the scintillator mechanism (STE stands for self-trapped excitons; CB stands for conduction band; VB stands for valence band; CL is for cross luminescence; adapted with permission from (Nikl, M. 2006).....	18
2.8 (a) A diagram showing how X-ray imaging is set up. (b) An X-ray image was created with a $Rb_2CuCl_3$ /PDMS scintillator and a 20-second exposure duration. (c) The intensity profile of the X-ray image with the contrast ratio is considered. The region of interest (ROI) is depicted here by the inserted green rectangle. (d) an X-ray image of a double-wire IQI with $Rb_2CuCl_3$ /PDMS scintillator and (e) with a $CaWO_4$ phosphor available in the marketplace. (f) Using the results from d) and (e), a plot of the resolution was constructed .....	19

## LIST OF FIGURES (Continued)

Figure	Page
3.1 Densitometer (Dietheim Limited, HR-200) .....	22
3.2 Abbe refractometer (ATAGO) with a sodium vapor lamp as a light source having wavelength of 589.3 nm (D line) with monobromonaphthalen as a contact layer .....	22
3.3 Powder X-ray Diffraction (Bruker D2 PHASER) .....	23
3.4 Picture of Agilent Cary 630 FTIR Spectrometer .....	25
3.5 (a) Block diagram of the UV-Vis NIR spectrometer.....	26
(b) Picture of UV-Vis-NIR spectrophotometer (Shimadzu, UV-3600).....	26
3.6 (a) Block diagram of PL process.....	26
(b) Picture of fluorescence spectrometer (Agilent technology Cary Eclipse).....	27
3.7 X-ray induced luminescence .....	27
3.8 Electroluminescent (Ocean Optics QE65 Pro spectrometer).....	28
4.1 Image of glass samples containing $27.5\text{Gd}_2\text{O}_3-(72.5-x)\text{B}_2\text{O}_3-x\text{Dy}_2\text{O}_3$ with various concentrations of $\text{Dy}_2\text{O}_3$ .....	29
4.2 X-ray diffraction pattern of 0.5 mol% $\text{Dy}_2\text{O}_3$ content glass .....	30
4.3 The refractive index relation of $27.5\text{Gd}_2\text{O}_3-(72.5-x)\text{B}_2\text{O}_3-x\text{Dy}_2\text{O}_3$ glasses doped with varying concentrations of $\text{Dy}_2\text{O}_3$ ions .....	31
4.4 FTIR transmittance spectra of prepared glasses.....	32
4.5 UV-Vis-NIR spectra of $27.5\text{Gd}_2\text{O}_3-(72.5-x)\text{B}_2\text{O}_3-x\text{Dy}_2\text{O}_3$ glass system .....	33
4.6 (a) Excitation spectra and (b) Emission spectra of $27.5\text{Gd}_2\text{O}_3-(72.5-x)\text{B}_2\text{O}_3-x\text{Dy}_2\text{O}_3$ glass system monitored at 275 nm (c) Emission spectra of $27.5\text{Gd}_2\text{O}_3-(72.5-x)\text{B}_2\text{O}_3-x\text{Dy}_2\text{O}_3$ glass system monitored at 350 nm .....	34
4.7 Diagrams depicting the transfer of energy from $\text{Gd}^{3+}$ ions to $\text{Dy}^{3+}$ ions.....	37
4.8 (a) The relationship between the emission intensity at 576 nm and the content of $\text{Dy}_2\text{O}_3$ in the prepared glass samples when excited at 275 nm (b) The relationship between the concentration of $\text{Dy}_2\text{O}_3$ in the produced glass samples and the emission intensity at 576 nm.....	37

## LIST OF FIGURES (Continued)

Figure	Page
4.9 The Decay time profile of $27.5\text{Gd}_2\text{O}_3-(72.5-x)\text{B}_2\text{O}_3-x\text{Dy}_2\text{O}_3$ glass system.....	38
4.10 Radioluminescence of $\text{Dy}_2\text{O}_3$ concentrations in $27.5\text{Gd}_2\text{O}_3-(72.5-x)\text{B}_2\text{O}_3-x\text{Dy}_2\text{O}_3$ (GBD) glasses.....	38
4.11 CIE coordinate diagram of $27.5\text{Gd}_2\text{O}_3-(72.5-x)\text{B}_2\text{O}_3-x\text{Dy}_2\text{O}_3$ glasses doped with varying concentrations of $\text{Dy}_2\text{O}_3$ .....	39
4.12 Schematic diagrams showing the Encapsulation of prepared glass on Blue LED.....	40
4.14 Encapsulation of studied glass with Blue LED. (a) Before encapsulation of glass with Blue LED (b), Blue LED powered with 3.0 volts (c) Glass encapsulated on Blue LED powered with 3.0 volts .....	40

# CHAPTER I

## INTRODUCTION

### 1.1 Background and motivation

When people first learned to manufacture fire, they also developed a desire for light. Because lighting currently plays a crucial role in people's daily lives and consumes 20% of the world's electricity (Schubert, E. F. et al., 2005), (Cho, J. et al., 2017). Numerous researchers, like Joseph Swan and Heinrich Goebel, have examined the development of light bulbs before the invention. However, light bulbs remained a scientific concept at that time. It was only feasible for commercial usage once Thomas Alva Edison received a patent for a carbon incandescent lamp in 1879. Another significant milestone in the development of lighting is the creation of light bulbs for commercial usage. An electric current was run through the filament until it heated up and released light by the incandescent principle. However, Edison's carbon-based filament lasts only about 13 hours and has a very short lifespan. Scientists then worked to create a filament to improve performance and service life until William Davis made a tungsten filament in 1910. Because of the filament's ability to withstand temperatures up to 3,000 degrees Celsius, tungsten filament lamps now last between 1,000 and 3,000 hours instead of just using 13 hours. A fluorescent light, commonly referred to as a gas lamp, was created in 1934. A gas lamp's basic operating concept is to drive the movement of the mercury gas, which emits heat and light, using electricity that flows through the starter and ballast. There is a wavelength of light that is harmful and has a spectrum that humans cannot see. Scientists developed a phosphorous coating to cover the surface of inner tubes. Create a fluorescent bulb, a type of phosphorescent phenomenon, to provide light next (Fluorescent).

This lamp uses less energy since it loses power as heat significantly less than incandescent lamps. A type of lamp with high potential and small size, lifespan, safety, and environmental protection entered the vision of scientists before the advent of

The inchoate semiconductor LED in the 1960s (Round, H. J., 1907; Holonyak, N., 1962; Craford, M. G., 1977).

In 1962, Nick Holonyak Jr. continued to advance this technology while employed by General Electric. Red LEDs were the first type of light-emitting diode. The first yellow LED and the red LED were created by M. George Craford, a graduate student at Holonyak. To exploit fiber optics in telecommunications, Thomas P. Pearsall created high brightness light-emitting diodes in 1976 (Holonyak, N., 1962; Craford, M. G., 1977). The first blue LED was created in 1979 by Shuji Nakamura of Nichia Corporation, but it took until 1994 to become economically viable for commercial use. Today, light-emitting diodes can be made in one or many colors. Since light-emitting diodes cost \$200 each initially, they were exclusively utilized as indicators in specialist laboratory equipment (Nakamura, S. et al., 1994). Through the use of a semiconductor chip for light emitting diodes, Fairchild Semiconductor lowered the price of individual LEDs to just 5 cents in the 1970s. LEDs for commercial devices have been successfully created by Fairchild, employing cutting-edge packaging techniques and chip fabrication procedures. Instead of incandescent bulbs, illuminated LEDs are utilized, and fluorescent lights provide brightness and energy efficiency benefits. Infrared LEDs are used in TV remotes, DVD players, other gadgets and calculators, clocks, lanterns, and other applications. We need wireless control, but its drawback is that it is costly and produces much heat.

Glass material has been used in various structural applications for centuries (Luewarasirikul, N. et al., 2018; Pawar, P. P. et al., 2016; Pawar, P. P. et al., 2017). Only the  $Dy^{3+}$  ions in the lanthanide group were of interest to the researcher because they have features that can be used in white light emission applications. Yellow light emission from the electric dipole (ED) corresponds to the intense radiation spectrum for  $Dy^{3+}$  ions at the  $4F9/2 \rightarrow 6H13/2$  transition (Ullah, I. et al., 2020; Wantana. N. et al., 2020). The other emission spectra signify a magnetic dipole's (MD) blue light emission at the  $4F9/2 \rightarrow 6H15/2$  transition. For choosing to employ unique borate-glass in this sculpture. The attractive optical and structural features (Kaur, S. et al., 2018; Ichoja, A. et al., 2018) and ease of fabrication in the literature analysis result in a relatively cheap manufacturing cost. Borate glass is a promising and excellent material for applications

such as nonlinear optics, detectors, and ionizing radiation transformers for the detection of electroluminescence. (Wantana. N. et al., 2020; Ichoja, A. et al., 2018). In addition, the compound gadolinium oxide, also known as  $Gd_2O_3$ , is an interesting component of the glass's overall make-up. In addition to having a linear solid glow with energy transfer behavior, it also has a high light yield due to its high atomic number (Wantana, N. et al., 2020; Shoaib, M. et al. 2020). Last, Gd/Dy co-doping in glass has been reported for photonic and scintillation applications (Wantana, N. et al., 2020). Developed lithium-aluminium-borate glasses doped  $Dy^{3+}$  for W-LED applications by (Rittisut, W. et al., 2021). For scintillation, materials can convert ionized radiation into visible photons. Furthermore, it has a variety of applications such as space exploration, industrial inspection security and medical radiography that obtain images with high resolution and efficiency from X-rays (A. Owens., 2008; D. Rinaldi. et al., 2020; Q. Chen. et al, 2018; X. Ou. et al., 2021)

The idea of the researcher is to create glass encapsulation in the form of a bell. Phosphors and epoxy resin are employed to encapsulate the LED, reducing the WLED structure to two layers as opposed to three. The structure's X-ray images still need to be reported in the  $Dy^{3+}$ -doped  $Gd_2O_3-B_2O_3$  X-ray imaging design. So, we'll develop the system and research the fundamentals of photography.

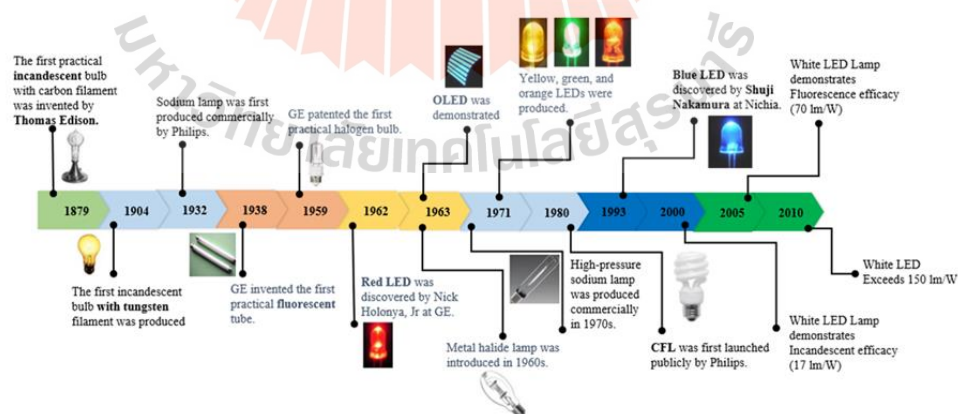


**Figure 1.1** The timeline of major discoveries in modern lighting technologies. (Adaptform: GE History, the history of the LED, OSRAM, and Lengthening the day)

This work will divide the study into two parts: 1. Design a new LED encapsulation 2. Design a luminescence system for X-ray imaging. We synthesize binary gadolinium borate glass doped with dysprosium ion from both of these. Therefore, we will use synthetic glass to determine its optical behavior, whether it is designing a blue LED to monitor light emissions before and after encapsulation. Including the creation of X-ray imaging systems for use in radiology or medical imaging areas.

## 1.2 Objectives of the thesis

The primary goal of this research was to explore the physical properties of the glass we synthesized and bring it to the composition  $27.5\text{Gd}_2\text{O}_3-(72.5-x)\text{B}_2\text{O}_3-x\text{Dy}_2\text{O}_3$  for applications in LED encapsulation and x-ray imaging. X-ray excitation luminescence (XEL), optical photoluminescence (PL), and electroluminescence (EL). The main aim of this thesis can be summarized as follows:

1.2.1 To synthesize  $27.5\text{Gd}_2\text{O}_3-(72.5-x)\text{B}_2\text{O}_3-x\text{Dy}_2\text{O}_3$  utilize Encapsulation in the Blue LED.

1.2.2 To compare the physical, optical, and emitting properties of  $\text{Dy}^{3+}$  ion-doped gadolinium borate glass by rapid melting and cooling technique.

1.2.3 To study the physical structure, including images obtained by X-ray stimulation.

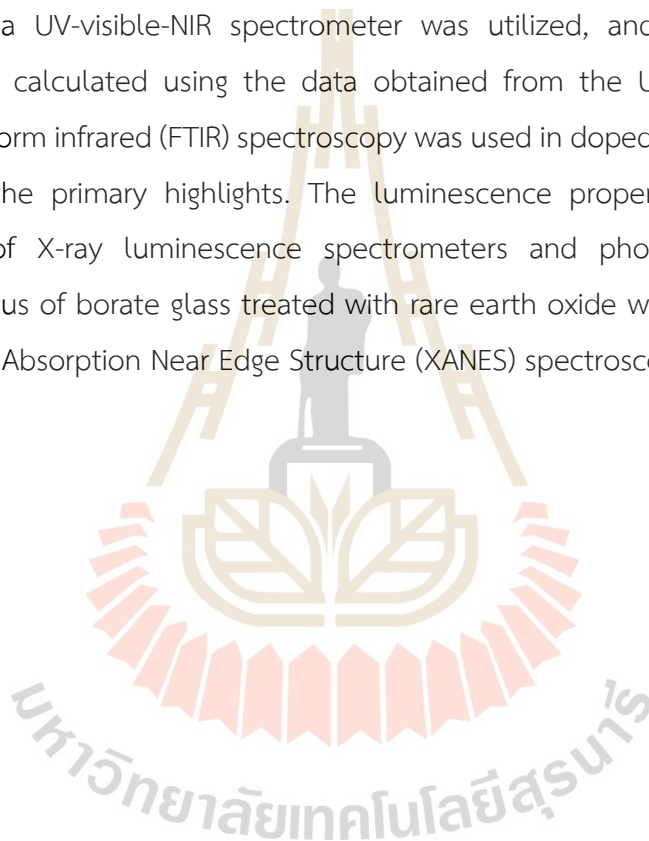
1.2.4 To analyze the mechanical properties and structure characteristics of  $27.5\text{Gd}_2\text{O}_3-(72.5-x)\text{B}_2\text{O}_3-x\text{Dy}_2\text{O}_3$  glasses series by using XRD, FTIR, Photoluminescence X-ray luminescence, Decay time and UV-Vis.

## 1.3 Outline of the thesis

In this study, a variety of gadolinium borate glass samples were made by mixing and melting the appropriate amounts of  $27.5\text{Gd}_2\text{O}_3-(72.5-x)\text{B}_2\text{O}_3-x\text{Dy}_2\text{O}_3$  glasses, where  $x$  is between 0.05 and 1.50 mol%, and the host matrix was prepared using the traditional melt quenching method. Doping was performed on the samples using both a single and a double dose of  $\text{Dy}^{3+}$  and trivalent rare-earth ions.

Using  $\text{Gd}_2\text{O}_3$ , trivalent rare earth oxide was incorporated into the borate to improve the host organization. Additionally, borate was used as a modifier to reduce

the hygroscopic qualities. To investigate the effect of the dopant on the structural, physical, chemical group, optical, photoluminescence, and radioluminescence properties of the material, the rare earth oxide from the  $Dy^{3+}$  series was chosen to serve as the dopant rare earth oxide. The estimations that were used came from a variety of sources. Initially, the Archimedes method was utilized to calculate the densities of the samples. The X-ray diffraction (XRD) measurement was carried out to validate the treated materials' original structure. To explore the optical features of the glass series, a UV-visible-NIR spectrometer was utilized, and the band gap was subsequently calculated using the data obtained from the UV-Visible-NIR spectra. Fourier-transform infrared (FTIR) spectroscopy was used in doped and undoped studies to regulate the primary highlights. The luminescence properties were under the supervision of X-ray luminescence spectrometers and photoluminescence. The oxidation status of borate glass treated with rare earth oxide was evaluated with the help of X-ray Absorption Near Edge Structure (XANES) spectroscopy.



## CHAPTER II

### THEORY AND LITERATURE REVIEWS

#### 2.1 Inorganic Light-Emitting Diodes (LEDs)

Although they have been investigated as possible options for blue LEDs for several years, semiconductors containing group II and VI elements have not succeeded. One example of such a semiconductor is ZnS/Se/ZnTe. Nevertheless, Nakamura and his colleagues were victorious in 1993. They decided to use InGaN, a material already demonstrating its potential in solid-state illumination (Nakamura, S. et al., 1997). Because the material is so chemically stable, producing epitaxial layers of sufficient quality for high-efficiency LED operation is challenging. This presents a challenge. On the other hand, the unusually high stability makes achieving exceptionally high current densities possible without damaging the LED material. The lumen package can be increased to values suitable for lighting applications (Figure 2.1). However, the fact that InGaN is relatively immune to flaws is arguably more significant. Standard InGaN LEDs have current densities that are noticeably higher than those that would be acceptable when utilizing other material combinations, such as AlGaAs ( $10^9$  cm<sup>-3</sup> to  $10^6$  cm<sup>-3</sup>). Still, because of InGaN slow surface recombination velocity, efficient LEDs can be built from dense layers of defects. This is because InGaN has a slower surface recombination velocity than other materials. Because of the development of long-lasting and dependable blue and UV LEDs, it is now possible to generate white light from solid-state devices by either externally combining the light from blue, green, and red LEDs or by color converting blue LEDs using phosphors.

In semiconductor device literature, the principle of LEDs is extensively described (Nakamura, S. et al., 1997; Zukauskas, A. et al., 2002; Sze, S. M. et al., 1981). Here, we will talk about using LEDs to produce white light and the pertinent characteristics of luminescent materials. Because color conversion is so necessary for

turning LEDs into sources of white light, this section devotes considerable space to discussing the phosphors themselves.



**Figure 1.1** LEDs with a traditional 5-millimeter diameter (on the left) and an LED with a high-power lighting (C. Ronda., 2008).

## 2.2 White and Colored LEDs

White light is often composed of a spectrum of colors rather than just one. Combining the blue and yellow/orange primary light sources is the quickest and easiest technique to produce a white light source (Figure 2.2). It may be difficult, at least in the case of small packages, to achieve homogenous mixing of the individual LEDs since the size of the small LED package places size constraints.

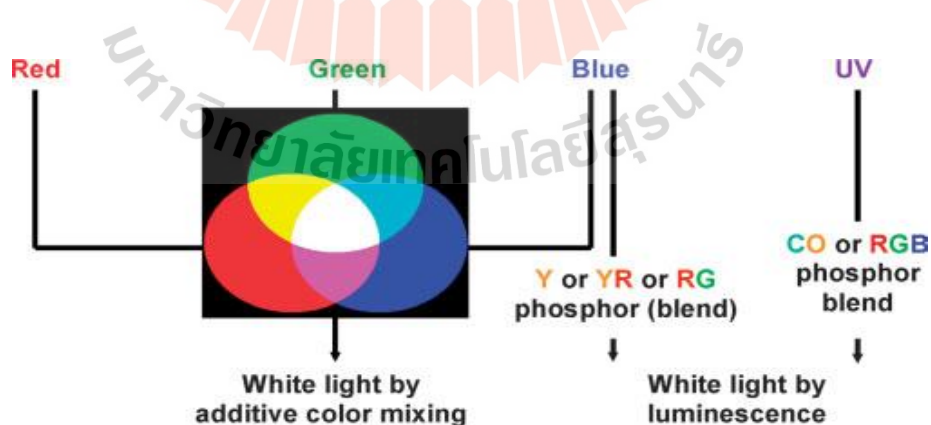


**Figure 2.2** Summary of different concepts to generate white light by primary light sources (C. Ronda., 2008).

The primary application for colored LEDs as light sources, as opposed to their employment in general illumination, is in settings that require the recreation of pure hues, such as those shown by the spectrum in Figure 2.3. Such environments include traffic signals and the brake or indicator lights on automobiles. In several application areas, filtered white incandescent light bulbs have been replaced by InGaN and AlGaInP LEDs as a result of the former technology's superior efficiency and longer lifetime.

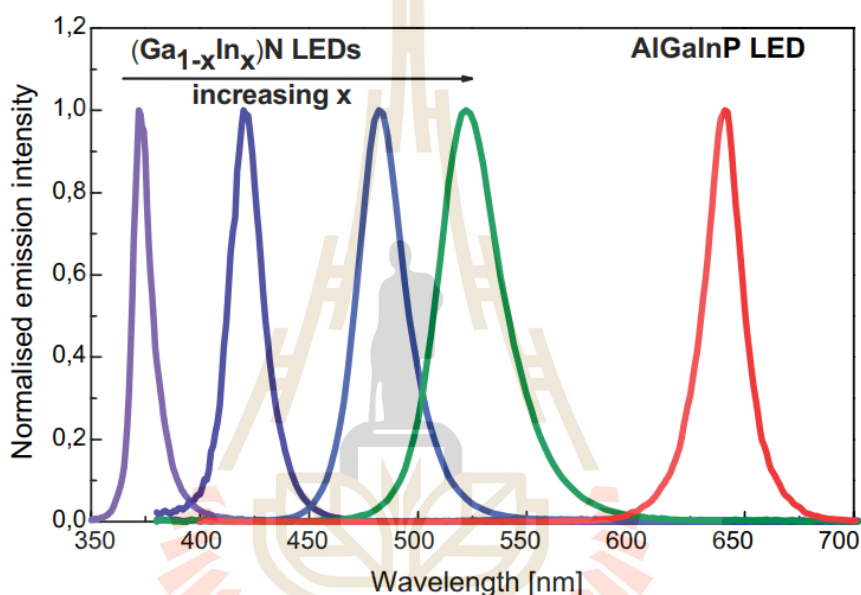


**Figure 2.3** The typical spectrum of a blue InGaN LED, a green InGaN LED, and a red AlGaInP LED (ranging from  $x = 0.0$  to about 0.45) (C. Ronda., 2008).

Because the material has a refractive index more significant than one, the crystal causes any light emitted at an angle more critical than the Brewster angle to be reflected into the crystal. The efficiency is yet decreased due to multiple internal reflections because some residual absorption is still present, such as at the metal contacts or the charge transportation layers. In the past, arranging the semiconductors on an LED so that they formed the shape of a truncated inverted pyramid allowed for the device to achieve the highest level of efficiency possible for a red light source (Figure 2.4). (Krames, M. R. et al., 1999).

This LED's internal and external efficiencies are anticipated to be close to 100%, resulting in a luminous efficiency of  $102 \text{ lm W}^{-1}$ . This figure demonstrates that light emitted by light emitting diodes (LEDs), which are currently the most efficient red-light source available on the market, have the potential to become the dominant source of light in the future.

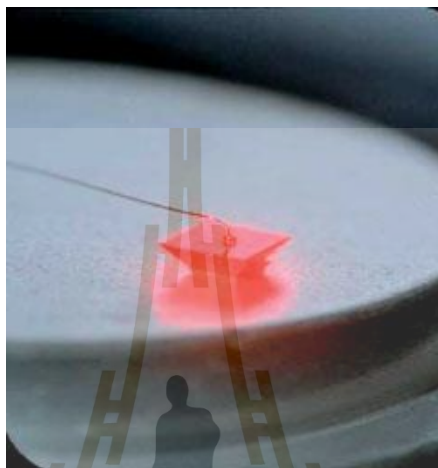


**Figure 2.4** InGaP LED shaped as a truncated inverted pyramid for efficient light extraction (Source: Lumileds).

### 2.3 Phosphor-Converted LEDs

The color point of these phosphor-converted LEDs (pcLEDs) is substantially impacted by the type of phosphor coating and that layer. Because of the high excitation density, which can be as high as  $30 \text{ W cm}^{-2}$  for a 1 W InGaN LED (chip area  $1 \text{ mm}^2$ , external efficiency around 30%), the phosphors that are used have to be able to absorb blue light significantly and have outstanding photochemical stability. The host lattice needs to have a high chemical and thermal stability level for the LED to have a lifetime of more than 10,000 hours (Scott, K., 2002). In addition, the phosphor should have a short decay time to stop saturation from occurring at high drive levels. Because of this, the LED spectrum will change or shift toward the color blue depending on the parameters of the drive. Consequently,  $\text{Eu}^{2+}$  and  $\text{Ce}^{3+}$  are activated when doped into stiff host lattices (oxides, nitrides, and sulfides), which are utilized in the most effective LED converter materials. The most popular phosphor is (Y,  $\text{Gd}_3\text{Al}_5\text{O}_{12}$ : Ce (YAG: Ce) (Nakamura, S. et al., 1997), The optical thickness of the phosphor coating

affects the effective color temperature of the light output from a phosphor-coated LED (pcLED). The first cool white LEDs had a luminous efficiency of roughly  $10 \text{ lm W}^{-1}$  (Bando, K. et al., 1998), translating to a light output of 0.7 lm at a power consumption of 70 mW. The phosphor used in these LEDs was YAG:Ce. As shown in Figure 2.2, the hues shift from a bluish white (cool white) to a yellowish white (warm white) as the layer thickness increases. A high-power LED with a rating of 5 W can generate up to 150 lm even though the efficiency of cool white LEDs is only  $30 \text{ lm W}^{-1}$  (Thornton, W. A. et al., 1971). Using a single yellow phosphor has the disadvantage of preventing the LED from producing low color temperatures (warm white light) with a high color rendering (Muller-Mach, R. et al., 2000). The LED spectrum does not contain any red light. In addition, the driving conditions affect the colors of cool white LEDs. These problems can be remedied using trichromatic white LEDs with two phosphors, the first of which emits light between 520 and 570 nm and the second between 590 and 660 nm.

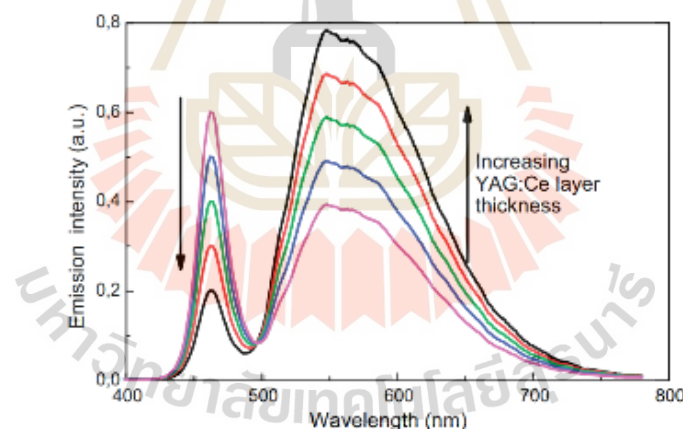


**Figure 2.5** Emission spectra of a white LED comprising a 460 nm-emitting blue InGaN chip and a phosphor as a function of the optical thickness of the YAG:Ce layer ( Rond, C. et al., 2008).

**Table 2.1** Comparison of advantages and disadvantages of LED (Abdelrahman, A. A. et al., 2016).

Advantages	Disadvantages
LED lighting can be fine-tuned to provide a diverse range of color temperatures because it is possible to combine multiple colored LED chips in the same array. The color temperature of the light produced by incandescent and halogen lamps is usually in the range of 2600K to 3000K, with 2700K being the most common of these values. Conversely, LEDs typically have color temperatures ranging from 2700K to 6000K or more.	LEDs are more expensive than other lights.
The efficiency of LEDs is undergoing rapid development at the moment.	There are situations when high voltage can cause LEDs to get damaged.
LEDs are more reliable.	Very little effectiveness across a vast area.
LEDs are more efficient to use under cold temperatures.	LEDs are responsible for reverse heat dissipation.

## 2.4 Composition of the present glass

Glass can be defined as "an inorganic product of fusion which has been cooled to a rigid condition without crystallization." The presence of long-range order in the crystal structure is the primary characteristic that differentiates crystals from glass. (Yamane and Asahara., 2000). The molten liquid is routinely cooled down to make glasses using this method. On the other hand, other techniques aren't used sparingly, such as chemical vapor deposition and the sol-gel process approach. Crystallization

may occur at a liquid's melting point ( $T_m$ ) if the liquid is cooled rapidly from a high temperature. If the crystallization occurs, there will be a sudden shift in the volume and enthalpy at the transition temperature. The heat capacity of the crystal will cause the volume and enthalpy to decline even further if the crystal is allowed to continue to cool after it has already been cooled. When a liquid is chilled below its melting point without crystallization, the resulting state is called a supercooled liquid. Within this zone, the liquid structure continued to reorganize itself even as the temperature fell; nevertheless, there was no sudden drop in volume or enthalpy due to a discontinuous rearrangement of the system (Varshneya., 1994).

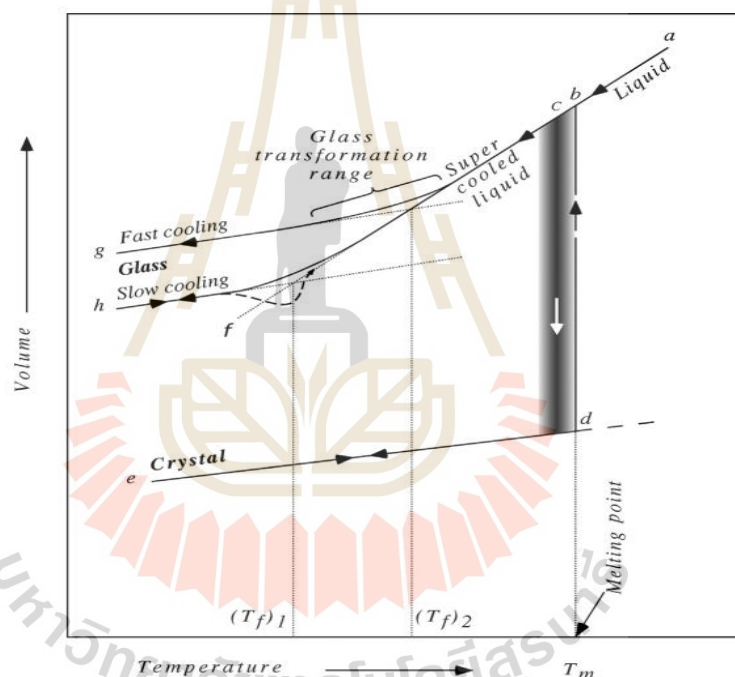


**Figure 2.6** The volume-temperature diagram for glass-forming liquid (Varshneya., 1994).

As the liquid is cold, the viscosity of the liquid increases. Because of the rise in thickness, the atoms will not be able to entirely reorganize themselves into the structure of the equilibrium liquid within the allotted amount of time for the experiment. The structure needs to catch up to what would be present if equilibrium were given enough time to develop. When the viscosity of the liquid is so high that its structure is fixed and independent of temperature, the enthalpy starts to deviate from the equilibrium line. It follows a curve with a gradually decreasing slope until the heat

capacity of the frozen liquid eventually determines it. The temperature area, also called the glass transformation region, is located between the boundaries where the enthalpy is that of the equilibrium liquid and that of the frozen solid. The glass transition temperature depends on the heating rate and the sample's prior thermal history. The frozen liquid has transformed into glass at this point. This process of changes in volume/enthalpy with temperature as a supercooled liquid is cooled through the glass transition region (Figure 2.6) (Varshneya, 1994)

In this research, we will focus on three types of glass in which the following components are combined: borate ( $B_2O_3$ ), gadolinium oxide ( $Gd_2O_3$ ), and dysprosium oxide ( $Dy_2O_3$ ) described below.

#### 2.4.1 Borate ( $B_2O_3$ )

Borate is a crucial component, mainly serving as a glass-forming agent and partially as a flux in the current glass components. The following is a synopsis of the twin roles that borate plays in the production and manufacturing processes: Borate was chosen as the material of choice for the current experiment for several apparent reasons, including the ease with which it is available, a low processing temperature, a low glass-forming temperature, and most crucially, its inexpensive cost. The advantage of tolerating extremely high  $Ln^{3+}$  concentrations is offset by the disadvantage that the material's luminous efficiency is decreased by having extremely high phonon energies. Borate is anticipated to work well as a host for  $Ln^{3+}$  activators when combined with other components in a stoichiometrically acceptable ratio.

#### 2.4.2 Gadolinium oxides ( $Gd_2O_3$ )

Gadolinium is particularly significant among the  $Ln^{3+}$  series because it might make transferring energy from the host to the activators and luminescence centers easier. Additionally, it might function as a modifier and effective sensitizer for the dopant  $Ln^{3+}$  in the current glasses. It does not emit visible light to the human eye, and its excitation ( $^8S_7 \rightarrow ^6G_J$ ) and emission ( $^6P_{7/2} \rightarrow ^8S_{7/2}$ ) occur in the ultraviolet spectrum. Nevertheless, it can produce visible emission in a host network through a process known as spectrum conversion or by being sensitized by another  $Ln^{3+}$  dopant. It has a more significant energy band gap, better thermal stability, and a higher permittivity (5.4 eV).

### 2.4.3 Dysprosium oxides ( $\text{Dy}_2\text{O}_3$ )

As a glass dopant and effective activator in the current glasses, Dy is a helpful element in the Lanthanides group. Dy has a crucial role in modifying glass and, consequently, in its luminosity. Dy doped glass luminescence requires extensive research in the visible and near-infrared spectrum. Due to the complex electronic structure's arrangement and tightly spaced energy levels, knowing dysprosium spectra was once thought to be essential. As a result, little attention has been given to dysprosium-induced luminescence. Nevertheless, if we pick the right host, we can get the essential  ${}^4\text{F}_{9/2} \rightarrow {}^6\text{H}_{13/2}$  and  ${}^4\text{F}_{9/2} \rightarrow {}^6\text{H}_{15/2}$  transitions from dysprosium. Although much work on spectral studies of  $\text{Dy}^{3+}$  ion-doped materials has been done, it is good optical.

## 2.5 Glass Forming Networks

In general, many elements can form to be glass when they are cooled from the molten state at a rate enough to prevent crystallization. The glass composition can be fundamentally classified into three types; (1) the network formers, (2) intermediates and (3) network modifiers.

### 2.5.1 Network formers

Glass network formers are the elements those form glasses on their own. Several oxides like  $\text{B}_2\text{O}_3$ ,  $\text{P}_2\text{O}_5$ ,  $\text{SiO}_2$ ,  $\text{TeO}_2$ , and  $\text{GeO}_2$  will readily form glass on cooling their melt. The oxides mentioned above compose the element with intermediate electronegativity. Thus, the nature of bonding is typically a mixture of ionic and covalent throughout the glass network.

### 2.5.2 Intermediate

Intermediate oxides will not form glass readily on their own. However, when mixed and melted with some of the glass-forming oxides, they encourage forming of a glass structure. Hence, they are called intermediates which contribute to the formation of glass in association with at least one glass former. Depending upon the network, they are a network former or modifier. T) the cation of intermediates occupies the positions of the glass former during the glass formation. Cations of

elements such as Zn, Ti, Pb, Be, Al, Zr, Th, and Cd act as intermediates in glass formation.

### 2.5.3 Network modifiers

When mixed with glass formers in appropriate proportions, some oxide elements like  $\text{Li}_2\text{O}$ ,  $\text{Na}_2\text{O}$ ,  $\text{K}_2\text{O}$ , and  $\text{CaO}$  change the properties of the glass. These ions are unable to build up a continuous network. Instead, they change the glass structure and hence, the named modifier. The network modifier cations locate randomly in the glass network whose position is close to the non-bridging anions like oxygen, halogens, etc.

## 2.6 Lanthanides

The trivalent state and comparable chemical behaviors distinguish the chemistry of rare earth (RE), abbreviated as RE. RE always occurs as natural mixes, making separating these elements more complicated than it would otherwise be. In the case of lanthanoids, this group exhibits several distinct changes compared to the main group components (Bartolo and Forte, Eds. 2006). The filling of 4f orbitals causes these differences. As can be seen in Table 2.2, the lanthanoids (Ln) are comprised of elements with an atomic number ranging from 57 to 71. In the case of trivalent lanthanoids ( $\text{Ln}^{3+}$ ), electron configurations take the form  $[\text{Xe}] 4f_n$  ( $n = 0-14$ ). In this configuration, the xenon core shows  $5s^2$  and  $5p^6$  filled orbitals, which are radially more external than 4f orbitals. The energy state of  $\text{Ln}^{3+}$  can be shown in a Dieke diagram (Bartolo and Forte, Eds. 2006).

**Table** Error! No text of specified style in document.1 Electron configuration of lanthanide elements and ions (Bartolo and Forte, Eds. 2006).

Atomic number	Element	Symbol	$\text{Ln}^{3+}$	Ground State
57	Lanthanum	La	$4f^0$	$^1S_0$
58	Cerium	Ce	$4f^1$	$^2F_{5/2}$
59	Praseodymium	Pr	$4f^2$	$^3H_4$
60	Neodymium	Nd	$4f^3$	$^4I_{9/2}$
61	Promethium	Pm	$4f^4$	$^5I_4$
62	Samarium	Sm	$4f^5$	$^6H_{5/2}$
63	Europium	Eu	$4f^6$	$^7F_0$
64	Gadolinium	Gd	$4f^7$	$^8S_{7/2}$
65	Terbium	Tb	$4f^8$	$^7F_6$
66	Dysprosium	Dy	$4f^9$	$^6H_{15/2}$
67	Holmium	Ho	$4f^{10}$	$^5I_8$
68	Erbium	Er	$4f^{11}$	$^4I_{15/2}$
69	Thulium	Tm	$4f^{12}$	$^3H_6$
70	Ytterbium	Yb	$4f^{13}$	$^2F_{7/2}$
71	Lutetium	Lu	$4f^{14}$	$^1S_0$

## 2.7 CIE Chromaticity Coordination and Color Correlated Temperature (CCT)

The light color perception by human eyes has frequently been studied using the CIE 1931 chromaticity system. The following equations are used to calculate the tristimulus color values X, Y, and Z as the first step in the process:

$$X = \int_{\lambda}^{\lambda'} \bar{x}(\lambda) P(\lambda) d\lambda \quad (2.1)$$

$$Y = \int_{\lambda}^{\lambda'} \bar{y}(\lambda) P(\lambda) d\lambda \quad (2.2)$$

$$Z = \int_{\lambda}^{\lambda'} \bar{z}(\lambda) P(\lambda) d\lambda \quad (2.3)$$

$P(\lambda)$  is power spectral density, and  $x$ ,  $y$ , and  $z$  are matching functions of color experienced by the eye. Then, chromaticity coordinates ( $x$ ,  $y$ , and  $z$ ) are evaluated utilizing relationships. (Jayasankar, Kumar, and Krishnaiah, 2013)

$$x = \frac{X}{X+Y+Z} \quad (2.4)$$

$$y = \frac{Y}{X+Y+Z} \quad (2.5)$$

$$z = \frac{Z}{X+Y+Z} \quad (2.6)$$

The Chromaticity Diagram's area can typically be plotted, and the emission color determined using only the color ( $x$ ,  $y$ ) coordinate.

## 2.7 Scintillation

When a substance is exposed to radiation, a chain of chemical reactions known as scintillation begins. Both the intrinsic lattice ion and the extrinsic impurities are changed as a direct consequence of this phenomenon. As a result of applying the Coulomb force during a charged particle's contact with matter, the charged particle will slow down due to its energy transfer to the electrons that make up the lattice. This process will continue until the particle has lost its power and ceased moving forward. When electromagnetic radiation interacts with matter, a quantum can either entirely or partially absorb the energy of the radiation. In either case, the situation results in the production of a highly energetic electron. Atoms will experience increased ionization and excitement as a result of this electron. The end consequence

will be secondary electrons and holes, which, in turn, will generate even more energetic versions of both electrons and holes. Last but not least, they will transmit their energy to the centers of luminosity.

Scintillation can be broken down into three distinct stages that occur in order. Figure 2.8 visually represents these steps (Birowosuto, 2007).

1. The process of converting the energy of an incoming radiation or particle into a large number of electron-hole pairs. This can be thought of as an energy transfer. This process involves the interaction of radiation with matter, the production of electrons and holes resulting from that interaction, their relaxation, and their subsequent thermalization.

2. The formation of defects and the mechanism of energy transfer that allows the energy of an electron-hole pair to be transferred to the luminous ion participating in the process.

3. The emission process occurs when the luminous ion returns to its ground state after being excited and emits radiation.

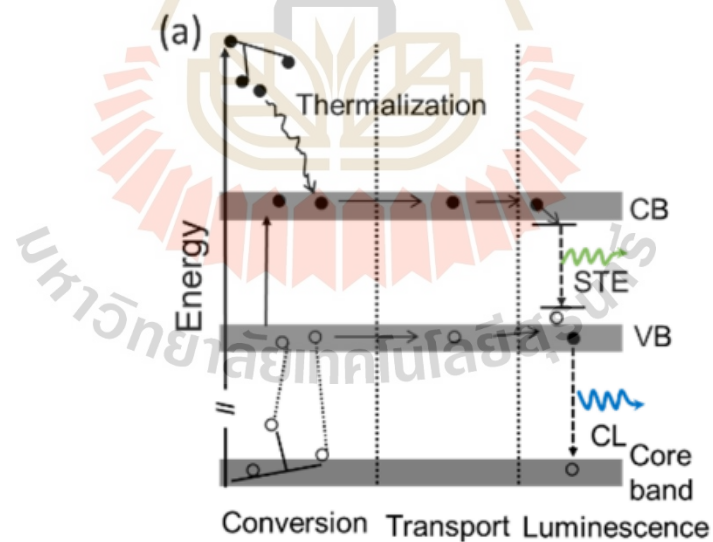


**Figure 2.7** A schematic representation of the scintillator mechanism (STE stands for self-trapped excitons; CB stands for conduction band; VB stands for valence band; CL is for cross luminescence; adapted with permission from (Nikl, M., 2006).

(Kopwitthaya, A. et al., 2022) Through the use of the cooling process, synthetic rubidium copper chloride-based flashes were successfully prepared. Depending on the wavelength of the stimulation, the  $\text{Rb}_2\text{CuCl}_3$  that is contained within the PDMS possesses a powerful emission of around 400 nm. The thermal stability has also been investigated using ionizing radiation and ultraviolet light. Fluorescence flashes demonstrate increased heat whenever the temperature is raised, and there is a specific temperature at which quenching is predominated. In the end, the x-ray images produced by our scintillator disclose particular information regarding the object. As shown in Figure 2.8, our research has resulted in developing of a potentially helpful and economically feasible flash phosphor for the X-ray screen business.

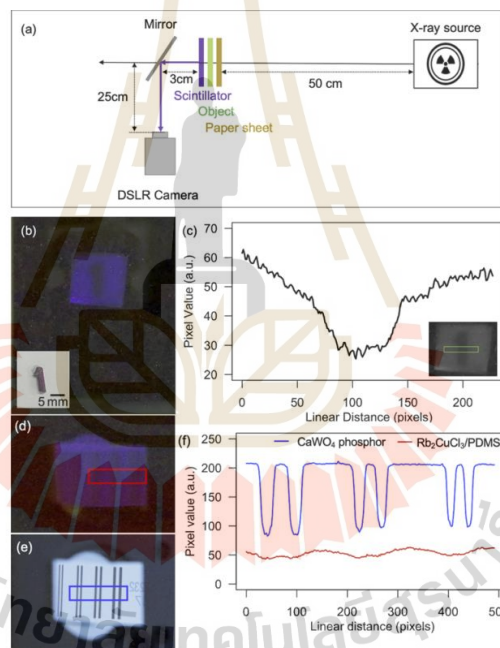


**Figure 2.8** (a) A diagram showing how X-ray imaging is set up. (b) An X-ray image was created with a  $\text{Rb}_2\text{CuCl}_3/\text{PDMS}$  scintillator and a 20-second exposure duration. The object seen in the inset is a piece of lead with a thickness of 2 millimeters. (c) The intensity profile of the X-ray image with the contrast ratio is considered. The region of interest (ROI) is depicted here by the inserted green rectangle. (d) an X-ray image of a double-wire IQI with  $\text{Rb}_2\text{CuCl}_3/\text{PDMS}$  scintillator and (e) with a  $\text{CaWO}_4$  phosphor available in the marketplace. (f) Using the results from (d) and (e), a plot of the resolution was constructed (Kopwitthaya, A. et al., 2022).

## CHAPTER III

### RESEARCH METHODOLOGY

#### 3.1 Sample preparation

##### 3.1.1 Preparation of Dy<sub>2</sub>O<sub>3</sub> doped (host glass)

The traditional melt quench method was utilized in the production of gadolinium borate glasses that had been doped with Dy<sup>3+</sup>. The chemical composition of these glasses was 27.5Gd<sub>2</sub>O<sub>3</sub>-(72.5-x) B<sub>2</sub>O<sub>3</sub>-xDy<sub>2</sub>O<sub>3</sub>, with the value of x ranging from 0.05, 0.10, 0.50, 1.00, and 1.50 mol%. As starting compounds, laboratory grades of the chemicals H<sub>3</sub>BO<sub>3</sub>, Gd<sub>2</sub>O<sub>3</sub>, and Dy<sub>2</sub>O<sub>3</sub> were utilized to produce this glass system. In an alumina crucible, melting was done in batches of roughly 15 grams each. (see Table 3.1)

**Table 3.1** Chemical composition of GdBdY glass.

Sample name	X (mol%)	Composition (mol%)
GdB0.05Dy	0.05	27.5Gd <sub>2</sub> O <sub>3</sub> -(72.5-0.05) B <sub>2</sub> O <sub>3</sub> -0.05Dy <sub>2</sub> O <sub>3</sub>
GdB0.10Dy	0.10	27.5Gd <sub>2</sub> O <sub>3</sub> -(72.5-0.10) B <sub>2</sub> O <sub>3</sub> -0.10Dy <sub>2</sub> O <sub>3</sub>
GdB0.50Dy	0.50	27.5Gd <sub>2</sub> O <sub>3</sub> -(72.5-0.50) B <sub>2</sub> O <sub>3</sub> -0.50Dy <sub>2</sub> O <sub>3</sub>
GdB1.00Dy	1.00	27.5Gd <sub>2</sub> O <sub>3</sub> -(72.5-1.00) B <sub>2</sub> O <sub>3</sub> -1.00Dy <sub>2</sub> O <sub>3</sub>
GdB1.50Dy	1.50	27.5Gd <sub>2</sub> O <sub>3</sub> -(72.5-1.50) B <sub>2</sub> O <sub>3</sub> -1.50Dy <sub>2</sub> O <sub>3</sub>

In an electrical furnace, the powder was heated to a temperature of 1400 °C Celsius for 3 hours. After that, the molten glass was spread out over a graphite plate, annealed at a temperature of 500 °C for three hours to remove thermal stress, and then cooled gradually to room temperature before being placed onto the polishers (1.00 × 1.50 × 0.30 cm<sup>3</sup>) to obtain a transparent sample with a thickness that was consistent throughout. The density of glass was initially determined using the Archimedes method, which involved the room-temperature immersion of water as the liquid medium.

After that, molar amounts were determined with the help of a sensitive microbalance with four digits (AND, HR 200). The glass sample's refractive index ( $n$ ) was determined with the assistance of an Abbe refractometer, a monobromonaphthalene ( $C_{10}H_7Br$ ) solution, and a sodium-vapor lamp serving as the light source. The FTIR spectrometer, model number Agilent-630, was used to research the chemical bonding within the glass matrix. A Shimadzu UV-3600 spectrophotometer is used to analyze the optical absorption spectra of polished samples between the wavelength ranges of 200 and 2000 nm. The photoluminescence (PL) spectra were acquired in the wavelength range of 200–800 nm and recorded at room temperature using a spectrofluorometer (Cary-Eclipse). The excitation light source was a xenon flashlight.

## 3.2 Physical properties

### 3.2.1 The density & Molar volumes

The density ( $\rho$ ) of the glasses, denoted by the symbol, was ascertained using Archimedes' method, in which water was taken to represent the immersion liquid. The apparatus for measuring density is depicted in Figure 3.1. This apparatus has a precision of 0.0001g. At room temperature, the sample was weighed using a balance in both air ( $W_a$ ) and water ( $W_w$ ), and the density was calculated using Equation (3.1).

$$\rho = \left[ \frac{W_a}{W_a - W_w} \right] \times \rho_b \quad (3.1)$$

Where  $W_a$  is the weight in the air,  $W_w$  is the weight in water and  $\rho_b$  is the density of water ( $\rho_b = 1 \text{ g/cm}^3$ ). The molar volume ( $V_m$ ) of glasses was computed with the help of density values that were brought in.

$$V_M = \frac{M_T}{\rho} \quad (3.2)$$

Where  $M_T$  is the glass's total molecular weight.



**Figure 3.1** Densitometer (Dietheim Limited, HR-200).

### 3.2.2 Refractive index

At a wavelength of 589.3 nm using a sodium lamp as a source and monobromonaphthalene as a contact liquid between the glass and the prism of the refractometer, the refractive indices ( $n$ ) of the glasses were determined with an Abbe refractometer with a measuring accuracy of 0.0001, as shown in figure 3.2. The accuracy of the measurement was shown to be 0.0001.



**Figure 3.2** A sodium vapor lamp was used as the light source for the Abbe refractometer (ATAGO), which had a wavelength of 589.3 nm (D line), and monobromonaphthalen was used as the contact layer.

### 3.3 Structural properties

Discovering the structure of glass samples is the focus of this dissertation, which uses X-ray diffraction, Fourier transform infrared spectroscopy, and X-ray absorption spectroscopy.

#### 3.3.1 X-ray diffraction

X-ray diffraction is an established method for characterizing materials and obtaining microstructural data for crystalline and non-crystalline materials. Information on crystal structure, lattice parameters, crystal size, composition, etc., might be obtained using this non-destructive technology and helpful for studying ceramics, metal alloys, semiconductors, polymers, and nanomaterials. To examine the glass structure, this experiment used a D2 Advance Bruker with Cu  $K\alpha$  and  $\lambda = 0.15406$  nm. The XRD patterns in the two ranges of  $10^\circ$  to  $80^\circ$  were recorded using a step size of  $0.02$  and a step time of  $0.4$ . The primary method for identifying the phase of a crystalline material and figuring out the size of a unit cell is X-ray diffraction (XRD). The crystalline sample affects X-ray diffraction, and X-ray tubes generate constructive interference of X-rays. Once it has been filtered to produce monochromatic X-rays, the model is the only object directed at—positive interference results from the sample's interaction with the incident radiation. W.L. Bragg provided the geometrical explanation of the XRD phenomena (constructive interferences). A photograph of an X-ray diffractometer can be found in figure 3.3.



Figure 3.3 Powder X-ray Diffraction (Bruker D2 PHASER).

### 3.4 Optical and spectral properties

#### 3.4.1 Fourier-transform infrared spectroscopy

Infrared analysis using the Fourier transform was performed on glasses to determine the contributions to the spectra made by each structural component and to emphasize the function of the lanthanide ions contained within the glass network. The Fourier transform infrared spectroscopy is one of the helpful technologies that can be used to resolve the structure of the local groupings in glasses. These non-destructive methods provide a comprehensive characterization of the structure as well as the vibrational properties of glasses. It has been discussed how to quantitatively interpret the absorption bands of an IR spectrum by using the value of the stretching force constant and the reduced mass of the vibrating cation-anion. The analysis of the IR absorption curves suggests that the coordination number is the most critical factor in determining the characteristics of the spectra. Infrared spectroscopy uses the fact that different types of molecules can absorb different frequencies due to the differences in their structures. These absorptions have resonance frequencies, which means that the frequency of the absorbed radiation is identical to that of the bond or group that is vibrating. The energies are affected in various ways, including by the masses of the atoms, the associated vibronic coupling, and the geometry of the molecular potential energy surfaces. When a harmonic oscillator can approximate the molecular Hamiltonian that corresponds to the electronic ground state near the equilibrium molecular geometry, the resonant frequencies in the Born-Oppenheimer and harmonic approximations are determined by the usual modes that correspond to the possible energy surface of the molecular electronic ground state. In particular, this is the case when a harmonic oscillator can approximate the molecular Hamiltonian corresponding to the electronic ground state. The first method, on the other hand, establishes a relationship between the resonant frequencies, the degree to which the connection is vital, and the mass of the atoms on each end of the association. Consequently, one particular bond form can be linked to a specific vibrational frequency.



**Figure 3.4** Picture of Agilent Cary 630 FTIR Spectrometer.

### 3.4.2 UV-Visible spectrophotometer

The absorption spectra were obtained by utilizing an ultraviolet-visible-near infrared (UV-VIS-NIR) spectrophotometer (Shimadzu, UV-3600) at room temperature to record spectra in the range of 200 nm to 2500 nm with a spectral resolution of 1 nm (figure 3.5). The spectrophotometer has three different types of excitation sources: a photomultiplier tube (PMT) for the ultraviolet (UV) region, a photomultiplier tube with an indium gallium arsenide (InGaAs) detector for the visible region, and an indium gallium arsenide (PbS) detector for the infrared (NIR) regions. Eq. (3.3) is the formula that Tauc proposed, and it may be used to theoretically predict the optical band gap and the direct and indirect transitions.

$$(\epsilon hv) = C(hv - E_g)^n \quad (3.3)$$

where C is a constant,  $\epsilon$  is molar extinction coefficient,  $E_g$  is the average band gap of the material and n depend on the type of transition. For  $n = 1/2$ ,  $E_g$  in equation (3.3) is direct allowed band gap (Tauc, J. et al., 1972).

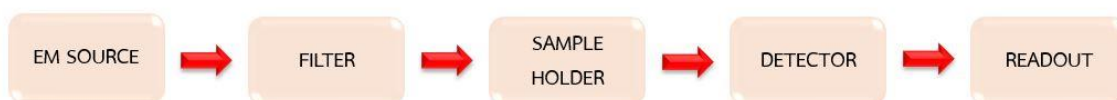


Figure 3.5(a) Block diagram of the UV-Vis NIR spectrometer.

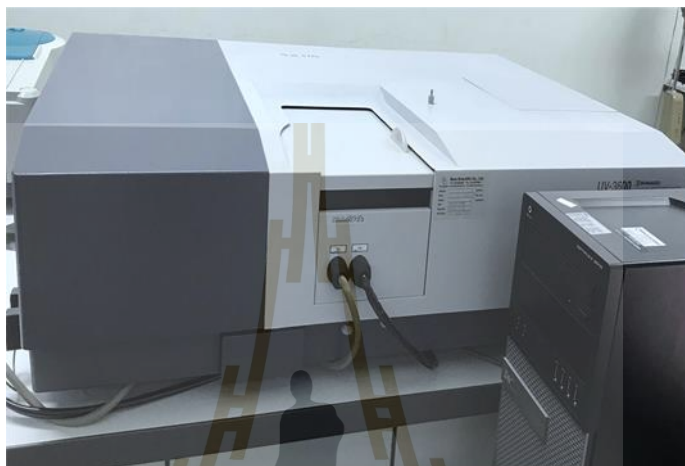


Figure 3.5(b) Picture of UV-Vis-NIR spectrophotometer (Shimadzu, UV-3600).

### 3.4.3 Photoluminescence technique

The emission, excitation and photoluminescence decay time of glass samples were recorded on a fluorescence spectrophotometer (Cary Eclipse) with Xe lamps as excitation sources and the block diagram of the luminescence spectrometer is displayed as shown in figure 3.6(a) and 3.6(b). The excitation and emission wavelength were monitored in region 200-1000 nm, performing the strongest emitting, were chosen to set value instrument for decay curve study. The strongest emission spectrum of each doped glass series was taken to analyze the emitting color via CIE 1931 chromaticity.

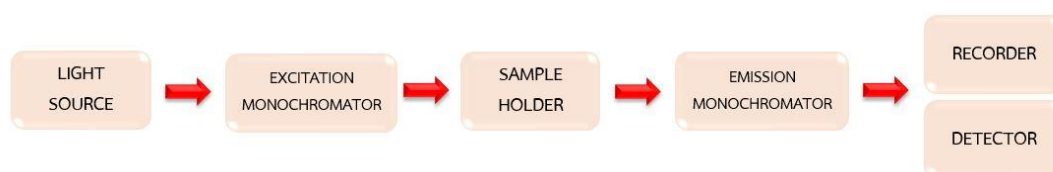


Figure 3.6(a) Block diagram of the PL process.



**Figure 3.6(b)** Picture of fluorescence spectrometer (Agilent technology Cary Eclipse).

#### 3.4.4 X-ray induced luminescence technique

The radioluminescence of the glass samples, also known as X-ray-generated optical luminescence, was also investigated at Nakhon Pathom Rajabhat University using a configuration of instruments specially designed for the purpose (figure 3.7). This apparatus includes a Cu target X-ray generator (Inel, RG3D), whose X-ray source was 50 kV and 30 mA, and a spectrometer (QE65 Pro, Ocean Optics) with an optical fiber to detect the emission spectra. The spectrometer was designed to detect the emission spectra.

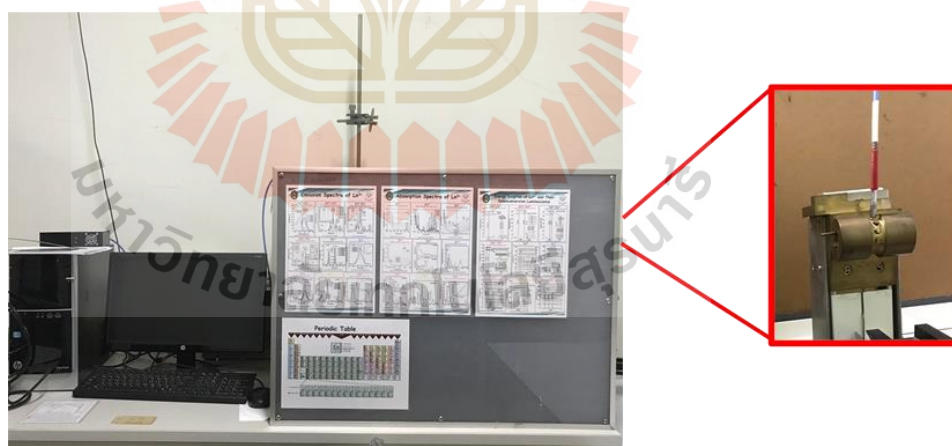


**Figure 3.7** X-ray induced luminescence.

#### 3.4.5 Electroluminescent

The light intensity emitted by the LEDs using the electroluminescent (Ocean Optics QE65 Pro spectrometer) is based on the specially designed instrumental setup in Nakhon Pathom Rajabhat University (figure 16). The principle of operation of the

machine is that when electricity is supplied from the power supply to the sample LEDs, the signal detector is checked and passed to the amplifier from will be processed and displayed on the computer.

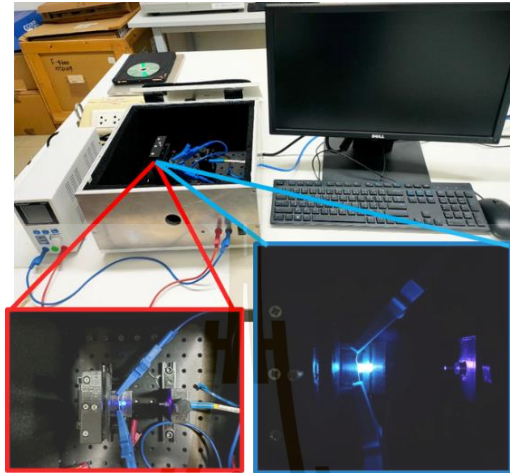


**Figure 3.8** Electroluminescent (Ocean Optics QE65 Pro spectrometer).



## CHAPTER IV

### RESULTS AND DISCUSSIONS

#### 4.1 $27.5\text{Gd}_2\text{O}_3-(72.5-x)\text{B}_2\text{O}_3-x\text{Dy}_2\text{O}_3$ glass system

The melt quenching technique was utilized to investigate the luminescence and physical properties of the gadolinium borate glasses that had been doped with  $\text{Dy}^{3+}$ .

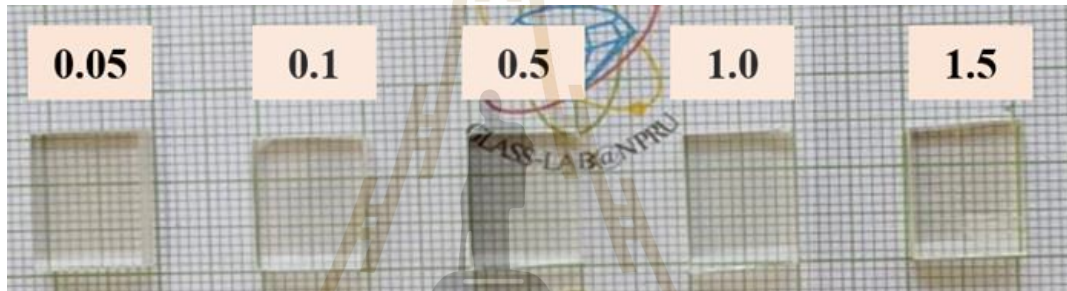


**Figure 4.1** Image of glass samples containing  $27.5\text{Gd}_2\text{O}_3-(72.5-x)\text{B}_2\text{O}_3-x\text{Dy}_2\text{O}_3$  with various concentrations of  $\text{Dy}_2\text{O}_3$ .

The photos in Figure 4.1 are of samples of optically polished GBD glass. The glass sample gradually goes from clear to light yellow as  $\text{Dy}_2\text{O}_3$  is added to it, as seen in the images (see Figure 4.1). Glass density is an essential characteristic to explore because of its wide range of variation in response to small changes in the glass structure. (Dias, J. D. M. et al., 2016; Kaewjaeng, S. et al., 2019).

##### 4.1.1 Structural properties of lass

Figure 4.2 shows that no distinct peaks are present, which is evidence that the nature of these glasses is amorphous.

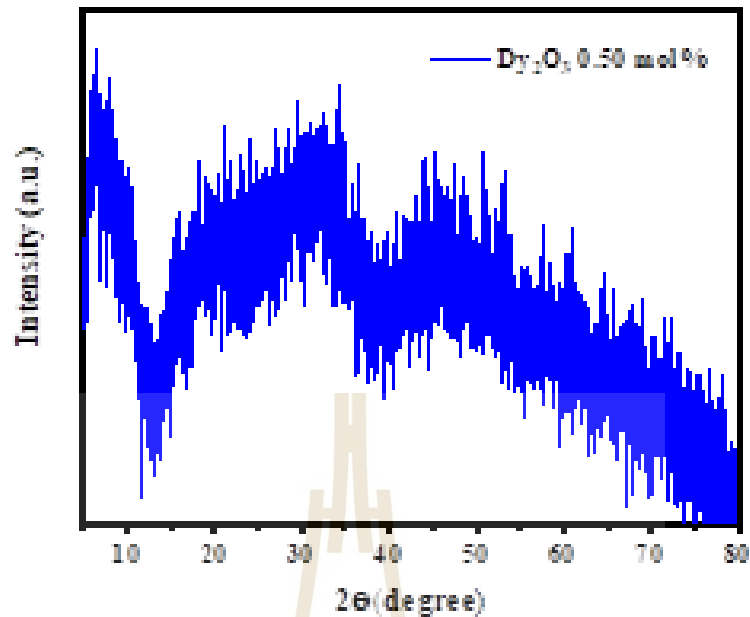


Figure 4.2 X-ray diffraction pattern of 0.5 mol% Dy<sub>2</sub>O<sub>3</sub> content glass.

#### 4.1.2 Physical properties

The primary source of knowledge regarding the structure and interactions of glass constituents is its physical properties. Therefore, precise measurement and exploration of these are required. All physical variables, including refractive indices ( $n$ ), molar volume ( $V_M$ ), and density ( $\rho$ ).

The values for density and molar volume are displayed in Table 4.1. These numbers have a non-linear trend, as can be seen. Using Kaewjaeng et al., the polarizability of oxide ions was assessed. We noticed a non-linear trend in our glass's density and molar volume. This indicates that the addition of Dy<sub>2</sub>O<sub>3</sub> content causes higher structural deterioration. Additionally, the molar volume is closely related to the oxygen distribution in the glass. (Umar, S. A. et al., 2017).

**Table 4.1** The density and molar volume results of  $27.5\text{Gd}_2\text{O}_3-(72.5-x)\text{B}_2\text{O}_3-x\text{Dy}_2\text{O}_3$  glass system.

Sample	Density	Average Density	Molar volume	Average Molar volume
	4.1180		36.5017	
0.05	4.1194	$4.1220 \pm 0.0058$	36.4889	$36.4659 \pm 0.0512$
	4.1287		36.4072	
	4.1632		36.1414	
0.10	4.1732	$4.1657 \pm 0.0066$	36.0546	$36.1197 \pm 0.0575$
	4.1607		36.1631	
	4.1943		36.1631	
0.50	4.1610	$4.1770 \pm 0.0167$	36.4525	$36.3136 \pm 0.1450$
	4.1756		36.3252	
	4.1328		37.0685	
1.00	4.1514	$4.1372 \pm 0.0126$	36.9019	$37.0289 \pm 0.1125$
	4.1274		37.1162	
	4.1940		36.8893	
1.50	4.2094	$4.1950 \pm 0.0140$	36.7542	$36.8808 \pm 0.1226$
	4.1815		36.9990	

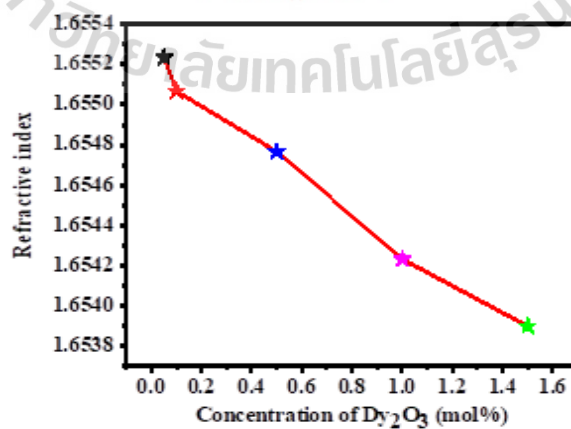


**Figure 4.3** The refractive index relation of  $27.5\text{Gd}_2\text{O}_3-(72.5-x)\text{B}_2\text{O}_3-x\text{Dy}_2\text{O}_3$  glasses doped with varying concentrations of  $\text{Dy}_2\text{O}_3$  ions.

As shown in Figure 4.3, the refractive index drops as the percentage of  $\text{Dy}_2\text{O}_3$  increases. The increased density of the glasses is responsible for the observed drop in the glasses' refractive index. (Zaman, F. et al., 2019).

#### 4.1.3 Fourier Transform Infrared Spectroscopy (FTIR)

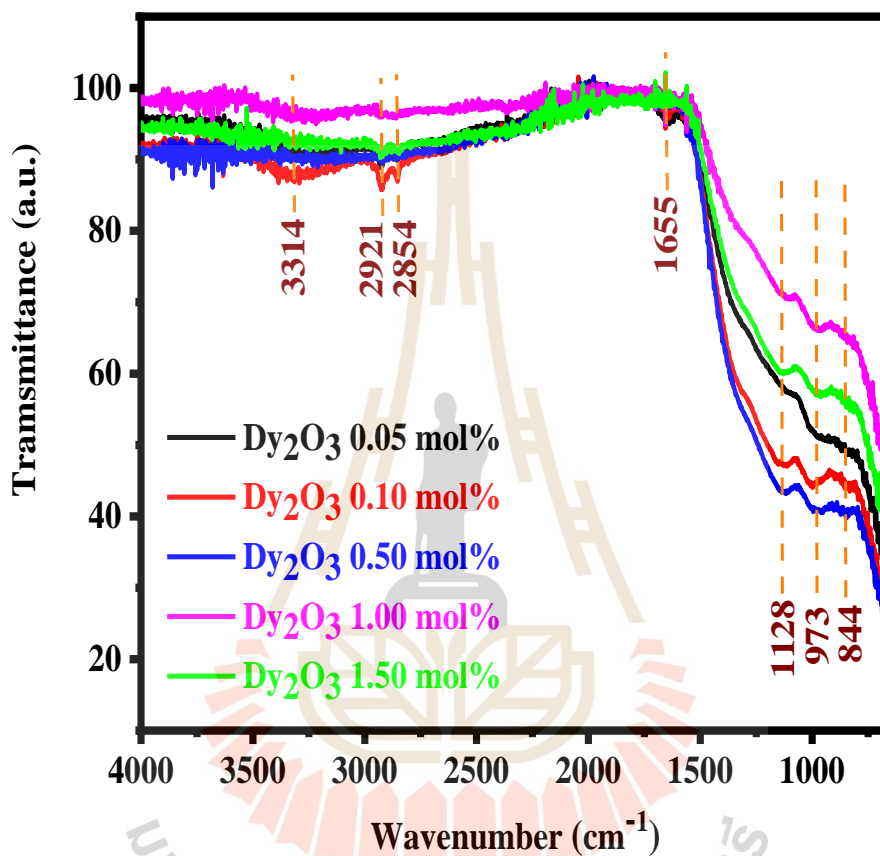


Figure 4.4 FTIR transmittance spectra of prepared glasses.

The FTIR band assignments of the obtained binary gadolinium borate glasses doped with  $\text{Dy}_2\text{O}_3$  content may be seen in Figure 4.4 and Table 4.2. The range of these band assignments is from 600 to 4000  $\text{cm}^{-1}$ .

**Table 4.2** FTIR band spectral allocations of the glass system composed of 27.5Gd<sub>2</sub>O<sub>3</sub>-(72.5-x) B<sub>2</sub>O<sub>3</sub>-xDy<sub>2</sub>O<sub>3</sub>.

Band position (cm <sup>-1</sup> )	Band Assignments
844	B–O bond stretching of tetrahedral BO <sub>4</sub> units (Balakrishna, A. et al., 2013)
973	B–O bond stretching of tetrahedral BO <sub>4</sub> units (Kaewjaeng, S. et al., 2021)
1128	B–O stretching vibrations of BO <sub>4</sub> units in tri-tetra and penta-borate groups (Lakshminarayana, G. et al., 2017)
1655	B–O bond stretching of trigonal BO <sub>3</sub> units (Venugopal, A. R. et al., 2021)
2854 - 3314	H–O–H water groups (Ravangvong, S. et al., 2019)

#### 4.1.4 UV-Vis-NIR Spectrophotometer

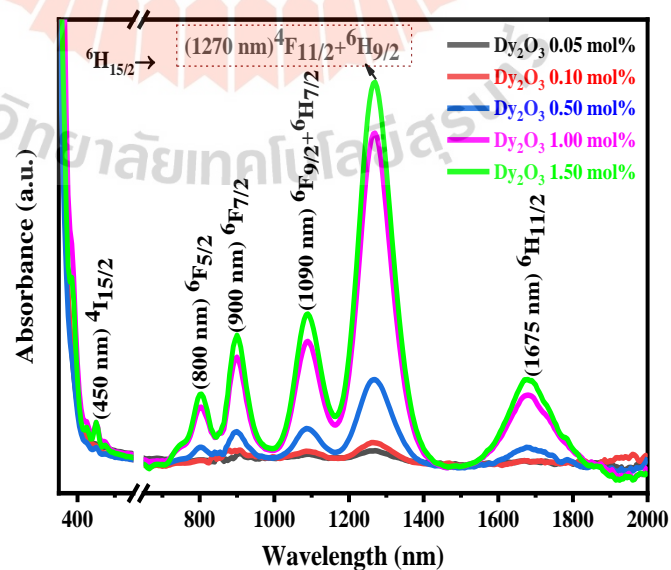


**Figure 4.5** UV-Vis-NIR spectra of 27.5Gd<sub>2</sub>O<sub>3</sub>-(72.5-x) B<sub>2</sub>O<sub>3</sub>-xDy<sub>2</sub>O<sub>3</sub> glass system.

Because of the transition from the ground state of  ${}^6\text{H}_{15/2}$  to several excited states, such as  ${}^4\text{I}_{15/2}$ ,  ${}^6\text{F}_{5/2}$ ,  ${}^6\text{F}_{7/2}$ ,  ${}^6\text{F}_{9/2}$ ,  ${}^6\text{H}_{7/2}$ ,  ${}^6\text{F}_{11/2}$  +  ${}^6\text{H}_{9/2}$  and  ${}^6\text{H}_{11/2}$ , respectively, the absorption spectra shown in Figure 4.5 exhibit dominant absorption peaks at 451, 800, 900, 1090, 1270, and 1675 nm. These peaks may be seen in the spectrum as 451, 800 (Luewarasirikul, N. et al., 2018)

#### 4.1.5 Absorption Spectra

Figure 4.6 a. Samples made entirely of glass showed the characteristic  $\text{Dy}^{3+}$  signal. We recorded 11  $\text{Dy}^{3+}$  ion peak crestings at 325, 350, 365, 387, 426, 452, and 472 nm and 4  $\text{Gd}^{3+}$  ion peak crestings at 246, 253, 275, and 313 nm in the current glasses.  $\text{Dy}^{3+}$  and  $\text{Gd}^{3+}$  ions were found to have the most significant excitation peaks at 350 nm and 275 nm, respectively. The  $\text{Dy}^{3+}$  ion was directly excited at 350 and 275 nm, respectively, to examine the emission spectra. We see  $\text{Gd}^{3+}$  ion emission at 311 nm for 275 nm excitation; this emission is only detectable up to 0.5 mol% of  $\text{Dy}_2\text{O}_3$ , after which there is no further emission.  $\text{Dy}^{3+}$  ion emission was seen at 481, 576, 663, and 753 nm. Beyond 0.5 mol%, the emission intensity diminishes as more  $\text{Dy}_2\text{O}_3$  content is added, with the highest emission intensity being reported for this content level. The concentration quenching effect is the cause of this decrease in intensity at high concentrations. (Rittisut W. et al., 2021)

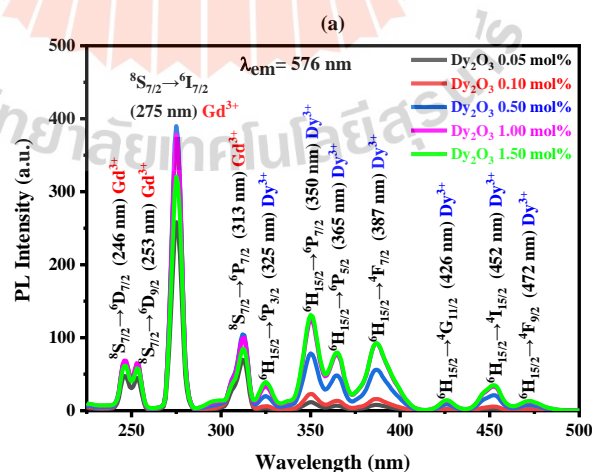


**Figure 4.6** (a) Excitation spectra, (b) Emission spectra of  $27.5\text{Gd}_2\text{O}_3-(72.5-x)\text{B}_2\text{O}_3-x\text{Dy}_2\text{O}_3$  glass system monitored at 275 nm and (c) Emission spectra of  $27.5\text{Gd}_2\text{O}_3-(72.5-x)\text{B}_2\text{O}_3-x\text{Dy}_2\text{O}_3$  glass system monitored at 350 nm.

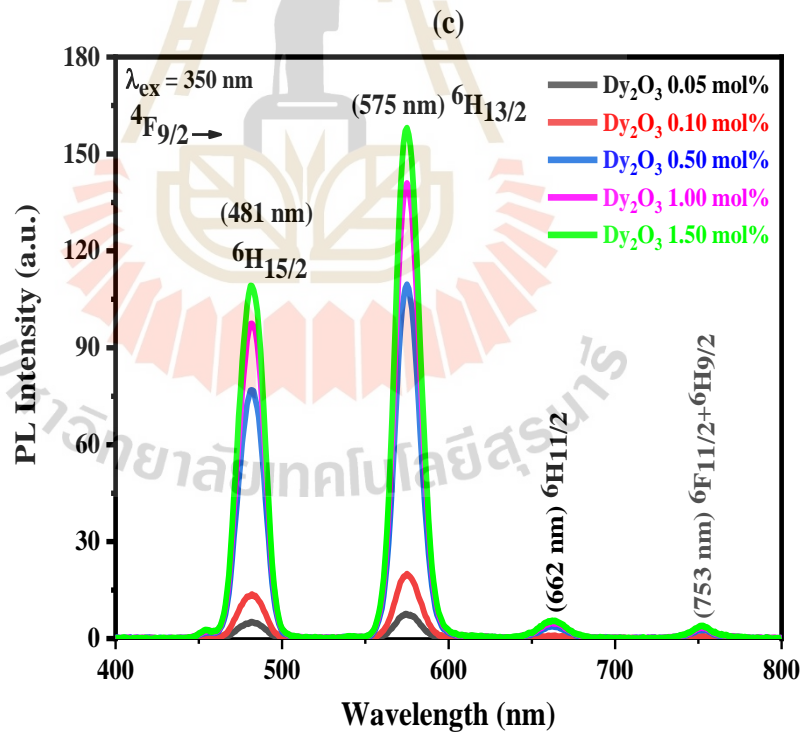
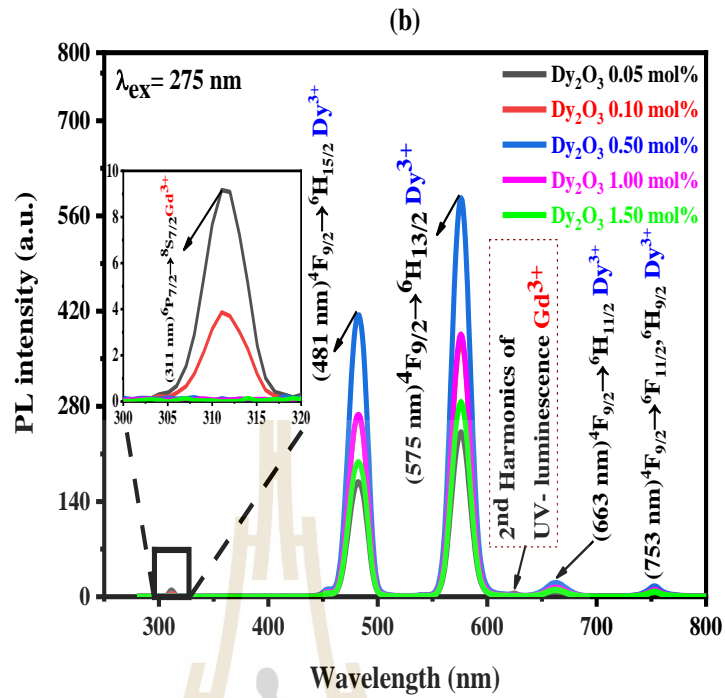


Figure 4.6 (Continued) (a) Excitation spectra, (b) Emission spectra of  $27.5\text{Gd}_2\text{O}_3-(72.5-x)\text{B}_2\text{O}_3-x\text{Dy}_2\text{O}_3$  glass system monitored at 275 nm and (c) Emission spectra of  $27.5\text{Gd}_2\text{O}_3-(72.5-x)\text{B}_2\text{O}_3-x\text{Dy}_2\text{O}_3$  glass system monitored at 350 nm.

#### 4.1.6 Energy Transfer

When examined at 275 nm of  $Gd^{3+}$  ions, Figure 4.7(b) demonstrates that energy transfer (ET) can be observed from the  ${}^6P_{7/2}$  transition of  $Gd^{3+}$  ions to the  ${}^6F_J$  levels of  $Dy^{3+}$  ions. This was found to be the case. In addition, the  ${}^6P_{7/2}$  to  ${}^8S_{7/2}$  transition of  $Gd^{3+}$  ions was observed to produce fluorescence at the wavelength of 311 nm. At a concentration of 0.5 mol%  $Dy_2O_3$ , concentration quenching was not observed. This was because it prevented the opening of cross-relaxation channels (CRC) and resonance energy transfer (RET) in the non-radiative transition. This is shown in Figure 4.8.

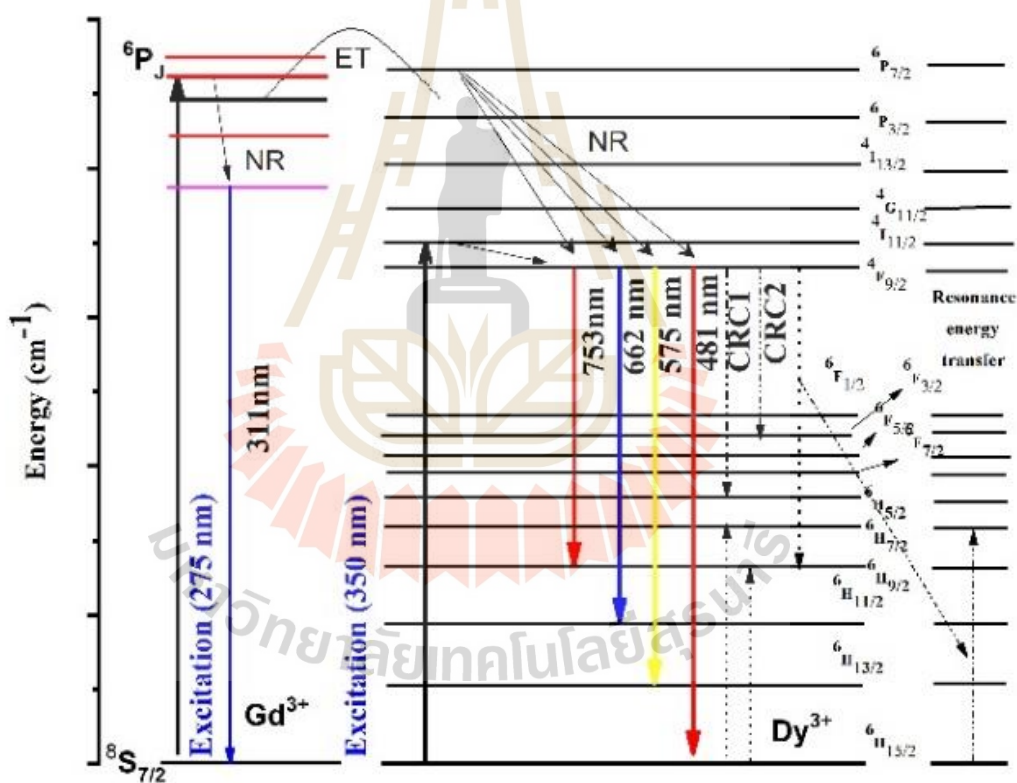
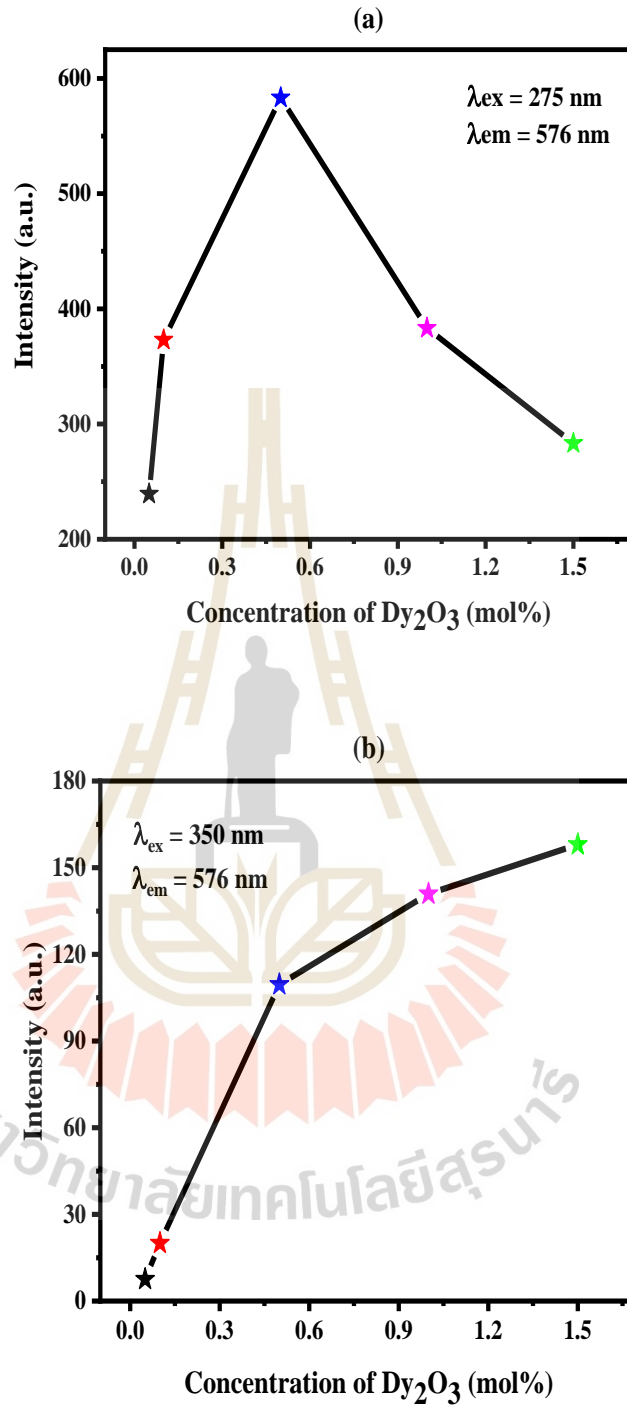


Figure 4.7 Diagrams depicting the transfer of energy from  $Gd^{3+}$  ions to  $Dy^{3+}$  ions.

#### 4.1.7 Photoluminescence excitation and emission (PLEs) spectra

Figures 4.9(a) and 4.9(b) illustrate the emission intensity (576 nm) of  $Dy_2O_3$  concentration at 275 nm and 350 nm excitations, respectively.



**Figure 4.8** (a) The relationship between the emission intensity at 576 nm and the content of  $\text{Dy}_2\text{O}_3$  in the prepared glass samples when excited at 275 nm and (b) The relationship between the concentration of  $\text{Dy}_2\text{O}_3$  in the produced glass samples and the emission intensity at 576 nm.

#### 4.1.8 Decay Time

The decay time profile depicted in Figure 4.10 exhibits single exponential behavior. The increased resonance energy transfer through cross-relaxation and resonant energy transfer was responsible for the observed drop in decay durations from 0.680 to 0.492 ms with increased  $\text{Dy}_2\text{O}_3$  content. (Zaman, F. et al., 2019).

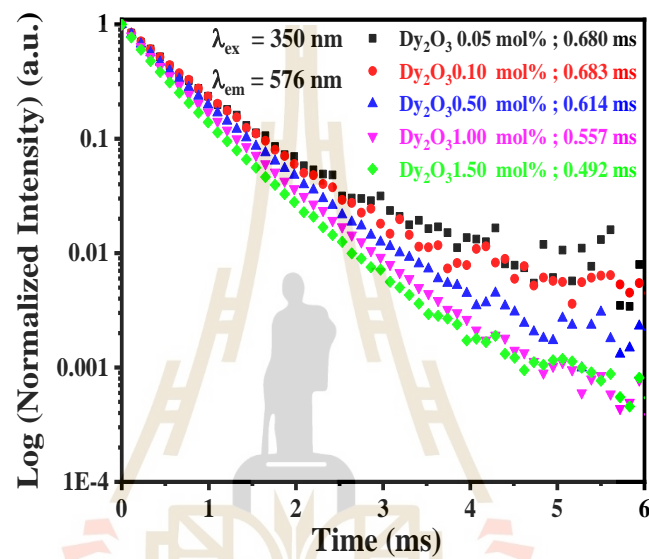


Figure 4.9 The Decay time profile of  $27.5\text{Gd}_2\text{O}_3-(72.5-x)\text{B}_2\text{O}_3-x\text{Dy}_2\text{O}_3$  glass system.

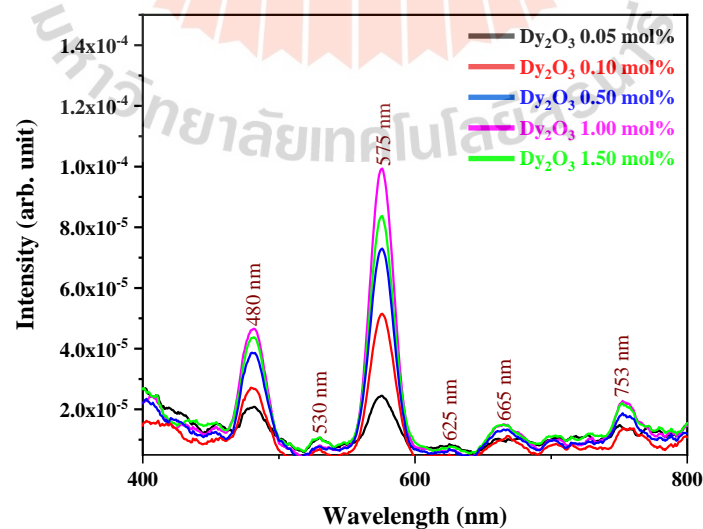
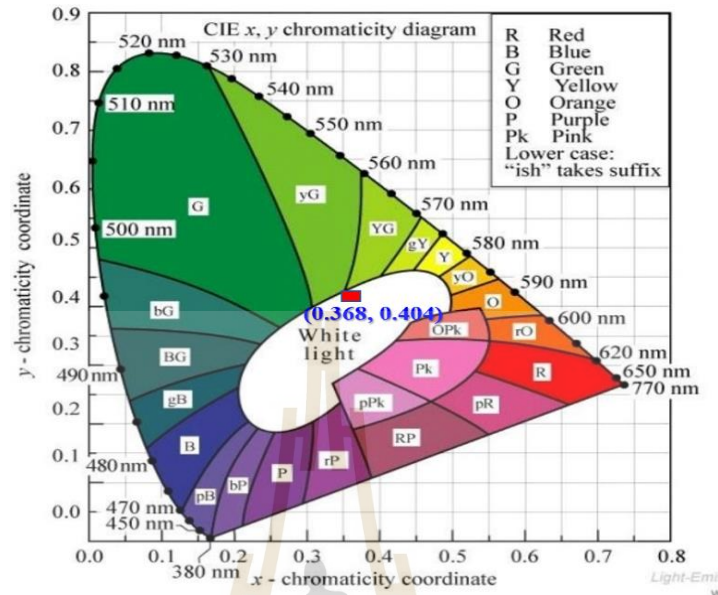


Figure 4.10 Radioluminescence of  $\text{Dy}_2\text{O}_3$  concentrations in  $27.5\text{Gd}_2\text{O}_3-(72.5-x)\text{B}_2\text{O}_3-x\text{Dy}_2\text{O}_3$  (GBD) glasses.

#### 4.1.9 CIE chromaticity coordinates and color correlated temperature (CCT)



**Figure 4.11** CIE coordinate diagram of  $27.5\text{Gd}_2\text{O}_3-(72.5-x)\text{B}_2\text{O}_3-x\text{Dy}_2\text{O}_3$  glasses doped with varying concentrations of  $\text{Dy}_2\text{O}_3$ .

Figure 4.12 illustrates the results, which show that the x and y color coordinates of the emission spectra of glasses doped with  $\text{Dy}_2\text{O}_3$  may be obtained from a precise location of about (0.368 and 0.404). The data illustrate this.

#### 4.1.10 Application of Blue LED Encapsulation

The CIE diagram demonstrated that the made glass sample emits white light with an excitation of 350 nm. This finding hints that the model may find application in white light emitting devices (WLEDs), also known as white light emitting diodes. Figure 4.13 is a diagram that illustrates the encapsulation of the studied glass into a UV (blue) LED. This diagram is in the form of a schematic. As can be seen, the color of light emitted by the glass is white, as shown in Figures 4.13(a)–4.13(c).

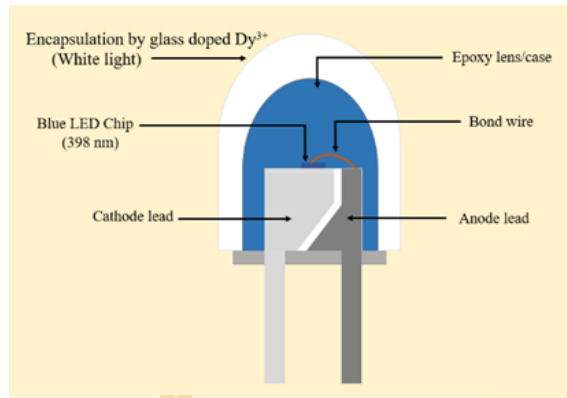


**Figure 4.12** Schematic diagrams showing the Encapsulation of prepared glass on Blue LED.

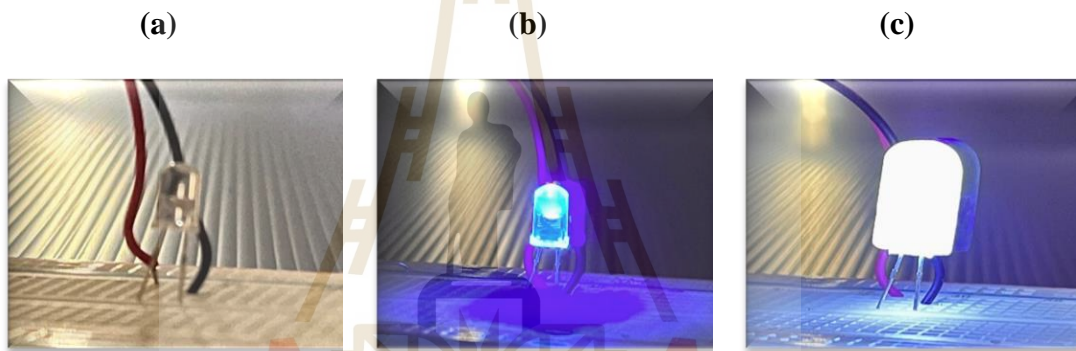


**Figure 4.13** Encapsulation of studied glass with Blue LED. (a) Before encapsulation of glass with Blue LED, (b) Blue LED powered with 3.0 volts and (c) Glass encapsulated on Blue LED powered with 3.0 volts.

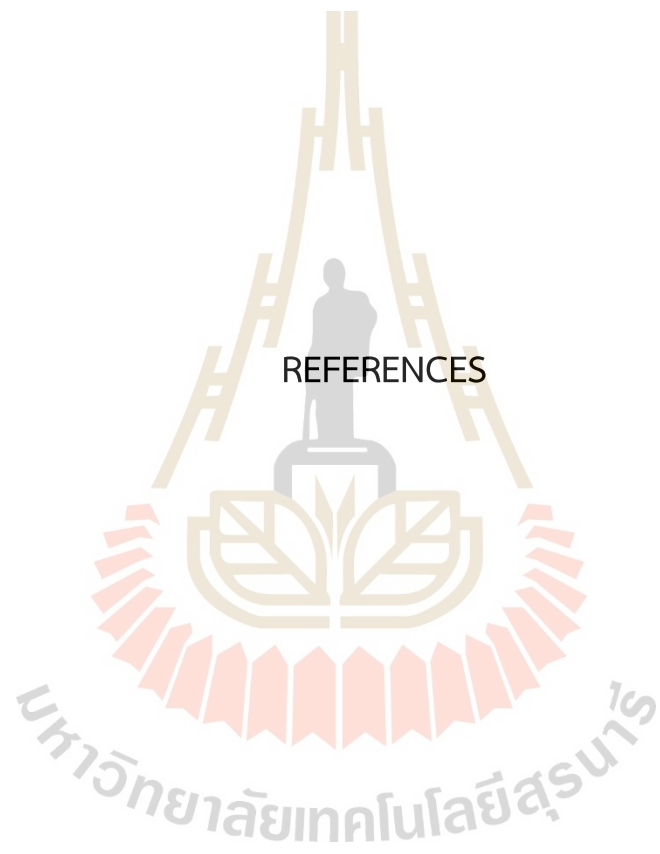
As can be seen in Figures 4.13 and 4.14, the bell-shaped glasses have been constructed by our team to encase a blue LED within them. As shown in Figure 4.14(a), the circuitry for the system was fabricated by connecting a breadboard rated for 3.0 volts to a blue LED. As shown in Figure 4.14(b), the connection was given an "on" switch to light the blue LED (398 nm). The encapsulation of a prepared bell-shaped glass sample is shown in Figure 4.14(c) on top of a blue LED. When the connection was turned "on," the LED lit up with a warm white light, suggesting that these glasses could be employed as encapsulating materials. (Shasmal, N. et al., 2019; Rajaramakrishna, R. et al., 2020; Boonpa, W. et al., 2022).

## CHAPTER V

### CONCLUSIONS

Using the time-honored method of melt-quenching, it was possible to successfully produce glasses with a composition of  $27.5\text{Gd}_2\text{O}_3-(72.5-x)\text{B}_2\text{O}_3-x\text{Dy}_2\text{O}_3$  (where  $x = 0.05, 0.1, 0.5, 1.0,$  and  $1.5$  mol%). The original encapsulating method will be the subject of this thesis study. According to the XRD spectra, these glasses have an amorphous structure. The photoluminescence and electroluminescence capabilities contributed to the white light emission demonstration. FTIR spectra were utilized to analyze the glasses' structural properties, and the results show distinct peaks associated with the borate network. It was discovered that  $\text{Dy}^{3+}$ -doped  $\text{Gd}_2\text{O}_3\text{-B}_2\text{O}_3$  glasses have emission spectra with the most incredible intensity at 0.5 mol% when monitored at 275 nm excitation and at 1.5 mol% when scanned at 350 nm excitation. When the  $\text{Dy}_2\text{O}_3$  content is considered, the temporal decay profile exhibits a lifespan that falls in the range of 0.680 to 0.492 ms. A white emission in the CIE 1931 color coordinate suggests these glasses may be suitable for encapsulating LEDs. To research electroluminescence, bell-shaped glasses containing blue LEDs were developed.

REFERENCES



## REFERENCES

- Abdelrahman, A. A., Kamelia, Y., and Ibrahim Y. (2016). Harmonics Monitoring Survey on LED Lamps, Volume 3 Issue 1, Special Issue, March 2017 - ISSN 2356-8569.
- Balakrishna, A., Rajesh, D., and Ratnakaram, Y. C. (2013). Structural and optical properties of Nd<sup>3+</sup> in lithium fluoro-borate glass with relevant modifier oxides, *Opt. Mater.* 35(12), 2670e2676.
- Boonpa, W., Kirdsiri, K., Kim, H. J., Rajaramakrishna R., and J. Kaewkhao, J. (2022). Dy<sup>3+</sup>-Doped Li<sub>2</sub>O: BaO: Gd<sub>2</sub>O<sub>3</sub>: SiO<sub>2</sub> Glasses for Luminescence Applications, *Integrated Ferroelectrics*, 224(1), 71-83.
- Bando, K. (1998). Symp. Proc. of the 8th Int. Symp. on the Sci. and Tech. of Light Sources, 80.
- Bowers B., and Anastas, P. (1998). Lengthening the day: a history of lighting technology: oxford university Press Oxford.
- Brodrick, J. (2016). DOE Solid-State Lighting R&D Plan, Department of Energy, Washington.
- Cho, J., Park, J. H., Kim, J. K., and Schubert, E. F. (2017). White Light-Emitting Diodes: History, Progress, and Future. *Laser Photonics Rev.* 11(2), 1600147.
- Craford, M. G. (1977). Recent Developments in Light-Emitting-Diode Technology. IEEE Trans. *Electron Devices*, 24(7), 935 – 943.
- Dias, J. D. M., Melo, G. H. A., Lodi, T. A., Carvalho, J. O., Façanha Filho, P. F., Barboza, M. J., Steimacher, A., and Pedrochi, F. (2016). Thermal and structural properties of Nd<sub>2</sub>O<sub>3</sub>- doped calcium boroaluminate glasses, *J. Rare Earths*. 34, 521–528.
- GE. (30 November). History. Available: <http://www.ge.com/about-us/history/1878-1904>
- Holonyak, N. Jr, and Bevacqua, S. (1962). Coherent (Visible) Light Emission from Ga (As<sub>1-x</sub>P<sub>x</sub>) Junctions. *Appl. Phys. Lett.* 1(4), 82– 83
- Huang, C. H. (Ed.). (2010). Rare Earth Coordination Chemistry, Fundamentals and Applications, John Wiley & Sons, Singapore.

- Ichoja, A., Hashim, S., Ghoshal, S. K., Hashim, I. H., and Omar, R. S. (2018). Physical, structural and optical studies on magnesium borate glasses doped with dysprosium ion, *J. Rare Earths*. 36, 1264–1271.
- J. M. P. J., Radielovic, D., and Vrenken, L. E. (1974). *J. Electrochem. Soc.* 121,1627.
- Kaewjaeng, S., Wantana, N., Kothan, S., Rajaramakrishna, R., Kim, H. J., Limsuwan, P., and Kaewkhao, J. (2021). *Radiation Physics and Chemistry*. 185, 109500.
- Kaewjaeng, S., Kothan, S., Chaiphaksa, W., Chanthima, N., Rajaramakrishna, R., Kim, H. J., and Kaewkhao, J. (2019). High transparency  $\text{La}_2\text{O}_3\text{-CaO-B}_2\text{O}_3\text{-SiO}_2$  glass for diagnosis x-rays shielding material application, *Radiation Physics and Chemistry*. 160, 41–47.
- Kaur, S., Vishwakarma, A. K., Deopa, N., Prasad, A., Jayasimhadri, M., and Rao, A. S. (2018). Spectroscopic studies of  $\text{Dy}^{3+}$  doped borate glasses for cool white light generation, *Mater. Res. Bull.* 104, 77–82.
- Krames, M. R., Ochiai-Holcomb, M., Höfler, G. E., Carter-Coman, C., Chen, E. I., Tan, I. H., and Collins, D. (1999). High-power truncated-inverted-pyramid  $(\text{Al}_x\text{Ga}_{1-x})_{0.5}$  In 0.5 P/GaP light-emitting diodes exhibiting > 50% external quantum efficiency. *Applied physics letters*, 75(16), 2365-2367.
- Lakshminarayana, G., Baki, S. O., Lira, A., Kityk, I. V., Caldiño, U., Kaky, K. M., and Mahdi, M. A. (2017). Structural, thermal and optical investigations of  $\text{Dy}^{3+}$ -doped  $\text{B}_2\text{O}_3\text{-WO}_3\text{-ZnO-Li}_2\text{O-Na}_2\text{O}$  glasses for warm white light emitting applications, *J. Lumin.* 186, 283–300.
- Luewarasirikul, N., and Kaewkhao, J. (2018).  $\text{Dy}^{3+}$ -doped Ba-Na-B White Light-Emit. Glass w-LED Appl.
- Müller-Mach, R., and Müller, G. O. (2000). *Proc. SPIE*, 3938, 30.
- Mishra, A. et al. (2004). Initial observation of magnetization hysteresis and quantum tunneling in mixed manganese-lanthanide single-molecule magnets, *J. Am. Chem. Soc.* 126(48),15648–15649.
- Nakamura, S., Mukai, T., and Senoh, M. (1994). Candela-Class High-Brightness Ingan/Algan Double-Heterostructure Blue-Light-Emitting Diodes. *Appl. Phys. Lett.* 64(13), 1687– 1689.

- Nakamura, S., and Fasol, G. (1997) *The Blue Laser Diode*, Springer, Berlin; Nakamura, S. MRS Bull. 29.
- Nikl, M. (2006). Scintillation Detectors for X-rays. *Meas. Sci. Technol.* 17, R37–R54.
- The history of the LED. Available:[http://www.osram.com/osram\\_com/news-and-knowledge/led-home/professional-knowledge/led-basics/led-history/index.jsp](http://www.osram.com/osram_com/news-and-knowledge/led-home/professional-knowledge/led-basics/led-history/index.jsp)
- Pawar, P. P., Munishwar, S. R., and Gedam, R. S. (2016). Physical and optical properties of Dy<sup>3+</sup> /Pr<sup>3+</sup> Co-doped lithium borate glasses for W-LED, *J. Alloy. Compd.* 660, 347–355.
- Pawar, P. P., Munishwar, S. R., Gautam, S., and Gedam, R. S. (2017) Physical, thermal, structural and optical properties of Dy<sup>3+</sup> doped lithium alumino-borate glasses for bright W-LED, *J. Lumin.* 183, 79–88.
- Ravangvong, S., N. Chanthima, N., Rajaramakrishna, R., Kim, H. J., Sangwaranatee, N., and Kaewkhao, J. (2019). *Solid state sciences.* 97, 105972.
- Rajaramakrishna, R., Ruangtaweep, Y., Sattayaporn, S., Kidkhunthod, P., Kothan, S., and Kaewkhao, J. (2020). *Radiation Physics and Chemistry.* 171, 108695.
- Round, H. J. (1907). A Note on Carborundum. *Electr. World*, 879.
- Rittisut, W., Wantana, N., Ruangtaweep, Y., Mool-am-kha, P., Padchasri, J., Rujirawat, S., Manyum, P., Yimnirun, R., Kidkhunthod, P., Prasatkhetragarn, A., Kothan, S., Kim, H.J. J., and Kaewkhao, J. (2021). Bright white light emission from (Gd<sup>3+</sup>/Dy<sup>3+</sup>) dual doped transparent lithium aluminum borate glasses for W-LED application, *Opt. Mater. (Amst.)*. 122, 111705.
- Shoib, M., Rajaramakrishna, R., Rooh, G., Chanthima, N., Kim, H. J., Saiyasombat, C., Botta, R., Nuntawong, N., Kothan, S., and Kaewkhao, J. (2020). Structural and luminescence study of Dy<sup>3+</sup> doped phosphate glasses for solid state lighting applications, *Opt. Mater. (Amst.)*. 109.
- Schubert, E. F., and Kim, J. K. (2005). Solid-State Light Sources Getting Smart. *Science.* 308:5726, 1274–8.
- Shasmal, N., and Karmakar, B. (2019). White light-emitting Dy<sup>3+</sup>-doped transparent chloroborosilicate glass: synthesis and optical properties, *J. Asian Ceram. Soc.* 7, 42–52.
- Sze, S. M. (1981). *Physics of Semiconductor Devices*, John Wiley & Sons.

- Scott, K. (May/June 2002) *The Lighting Journal*, 34.
- Thornton, W. A. (1971). *J. Opt. Soc. Amer.* 61, 1155; Koedam, M. and Opstelten, J. *Lighting Research and Technology*, 3, 205.
- Ullah, I., Shah, S. K., Rooh, G., Srisittipokakun, N., Khan, A., Kaewkhao, J., Kim, H. J., and Kothan, S. (2020). Spectroscopic study and energy transfer behavior of  $Gd^{3+}$  to  $Dy^{3+}$  for  $Li_2O-MgO-Gd_2O_3-B_2O_3-Dy_2O_3$  glasses for white emission material, *J. Lumin.* 226.
- Umar, S. A., Halimah, M. K., Chan, K. T., and Latif, A. A. (2017). Physical, structural and optical properties of erbium doped rice husk silicate borotellurite (Er-doped RHSBT) glasses, *J. Non. Cryst. Solids.* 472, 31–38.
- Venugopal, A. R., Rajaramakrishna, R., Rajashekhara, K. M., Rajaguguk, J., Ayachit, N. H., Kothan, S., and Kaewkhao, J. (2021). *Journal of Non-Crystalline Solids.* 554, 120604.
- Wantana, N., Ruangtaweep, Y., Kaewnuam, E., Kang, S. C., Kim, H. J., Kothan, S., and J. Kaewkhao, J. (2020). Development of  $WO_3-Gd_2O_3-B_2O_3$  high density glasses doped with  $Dy^{3+}$  for photonics and scintillation materials application, *Solid State Sci.* 101.
- Zaman, F., Rooh, G., Srisittipokakun, N., Ahmad, T., Khan, I., Shoaib, M., Atallah., Rajaguguk, J., and Kaewkhao, J. (2019). Comparative investigations of Gadolinium based borate glasses doped with  $Dy^{3+}$  for white light generations, *Solid State Sci.* 89, 50–56.
- Zukauskas, A., Shur, M. S., and Caska, R. (2002). Introduction to Solid-State Lighting, John Wiley & Sons. 122.

## CURRICULUM VITAE

Name: Mr. Atcharyasart Phongsa

Date of Birth: August 3, 1990

Place of Birth: KhonKaen Thailand

Education Background:

2009-2013 B.Sc. (Physics) Khon Kean University, Khon Kean, Thailand

2013-2016 M.Sc. (Applied Physics) Chiang Mai University, Chiang Mai, Thailand.

2016 – 2022 Ph.D. candidate (Applied Physics), Suranaree University of Technology, Nakhon Ratchasima, Thailand

### Publication

A. Phongsa., et al. (2022). White emission from  $Dy^{3+}$  doped  $Gd_2O_3-B_2O_3$  glass for WLEDs encapsulation, *Optik*, 265-169532



มหาวิทยาลัยเทคโนโลยีสุรนารี